Chlorine-rich metasomatic H2O-CO2 fluids in amphibole-bearing peridotites from Injibara (Lake Tana region, Ethiopian plateau): nature and evolution of volatiles in the mantle of a region of continental flood basalts.

Chlorine-rich metasomatic H_2O-CO_2 fluids in amphibole-bearing peridotites from Injibara (Lake Tana region, Ethiopian plateau): nature and evolution of volatiles in the mantle of a region of continental flood basalts

Maria Luce Frezzotti[1], Simona Ferrando[2], Angelo Peccerillo[3], Maurizio Petrelli[3], Francesca Tecce[4] and Andrea Perucchi[5]

[1] Department of Earth Sciences, University of Siena, Via Laterina 8, 53100 Siena, Italy. *frezzottiml@unisi.it*

[2] Department of Mineralogical and Petrological Sciences, University of Torino, Via V. Caluso 35, 10125 Torino, Italy.

[3] Department of Earth Sciences, University of Perugia, P.zza Università 1, 06100 Perugia, Italy.

[4] IGAG - CNR, c/o Department of Earth Sciences, University Roma 1 – La Sapienza, P.za A. Moro 5, 00185 Roma, Italy.

[5] Sincrotrone ELETTRA, Trieste, 34012 Basovizza (Trieste), Italy.

Abstract

Petrological and geochemical study of volatile bearing phases (fluid inclusions, amphibole, and nominally anhydrous minerals) in a spinel lherzolite xenolith suite from Quaternary lavas at Injibara (Lake Tana region, Ethiopian plateau) shows compelling evidence for metasomatism in the lithospheric mantle in a region of mantle upwelling and continental flood basalts. The xenolith suite consists of deformed (i.e., protogranular to porphyroclastic texture) Cl-rich pargasite lherzolites, metasomatized (LILE, and Pb enrichment in clinopyroxene and amphibole) at $T \leq 1000°C$. Lherzolites contain chlorine-rich H_2O-CO_2 fluid inclusions, but no melt inclusions. Fluid inclusions are preserved only in orthopyroxene, while in olivine, they underwent extensive interaction with host mineral. The metasomatic fluid composition is estimated: $X_{CO2} = 0.64$, $X_{H2O} = 0.33$, $X_{Na} = 0.006$, $X_{Mg} = 0.006$, $X_{Cl} = 0.018$, (salinity = 14 - 10 NaCl eq. wt. %, $a_{H2O}= 0.2$, Cl = 4-5 mole %). Fluid isochores correspond to trapping pressures of 1.4 - 1.5 GPa or 50 -54 km depth (at T = 950°C). Synchrotron sourced micro-infrared mapping (ELECTRA, Trieste) shows gradients for H_2O distribution in nominally anhydrous minerals, with considerable enrichment at grain boundaries, along intragranular microfractures, and around fluid inclusions. Total water amounts in lherzolites are variable from about 150 up to 400 ppm. Calculated trace element pattern of metasomatic fluid phases, combined with distribution and amount of H_2O in nominally anhydrous minerals, delineate a metasomatic Cl-, and LILE-rich fluid phase heterogeneously distributed in the continental lithosphere. Present data suggest that Cl-rich aqueous fluids were important metasomatic agents beneath the Ethiopian plateau, locally forming high water content in the peridotite , which may be easily melted. High Cl, LILE, and Pb in metasomatic fluid phases suggests the contribution of recycled altered oceanic lithosphere component in their source.

Keywords: peridotites, Cl,H_2O, mantle metasomatism, Ethiopian plateau, large igneous province

1. INTRODUCTION

C-O-H-S and halogens present in the Earth's upper mantle in different physical states (i.e. free fluid[1] phases, dissolved in melts, in interstitial solid solutions, as well as stored in nominally anhydrous minerals) play a fundamental role in mantle properties and processes, including rheology, metasomatism, and melting (e.g., Wallace and Green, 1988; Thompson, 1992; Green and Falloon, 1998; Wyllie and Ryabchikov, 2000; Dasgupta and Hirschmann, 2006).

Fluid inclusions in xenolith suites provide an important opportunity to characterize free fluid phases at depth (cf., Andersen and Neumann, 2001 for a review). Since E. Roedder's first studies (1965), it has been evident that CO_2 dominate in the lithospheric mantle (< 2-3 GPa). Overwhelming CO_2, however, is not the sole component in mantle fluid inclusions. H_2O-bearing CO_2 inclusions have been reported in peridotites from subduction-zones (e.g., Schiano et al., 1995), and, more recently, from Canary and Hawaii intraplate oceanic settings (Frezzotti et al., 2002a and b; Frezzotti and Peccerillo, 2007), revealing a major role for aqueous fluid phases also in zones of intraplate mantle upwelling. At Tenerife (Canary Islands), Frezzotti et al. (2002a) suggested a chlorine-rich composition for aqueous fluids, based on the presence of reaction rims of talc + carbonate + halite lining fluid inclusions. However, a quantification of the halogen (e.g. chlorine) content of aqueous fluid phases at lithospheric depths by fluid inclusion study is missing. Yet, such an information would be of particular interest to trace the H_2O exchanges between Earth's reservoirs, since chlorine is water-soluble and behaves incompatibly. In contrast, at higher pressures, above 4-5 GPa, a high Cl activity in aqueous fluids is testified by hydro-saline fluids (Cl about 12 - 50 mol. %) in sub-micrometer sized inclusions in diamonds (Navon et al., 1988; Izraeli et al., 2001; Klein-BenDavid et al., 2004; 2007) .

Present study aims to provide a better understanding of the role of volatiles in the lithosphere of a region of continental mantle upwelling and formation of large igneous provinces (LIP's). LIP's are traditionally interpreted as melting products of plume heads (White and McKenzie, 1995; Condie, 2001; Ernst and Buchan, 2003), although the relative lithospheric – plume contribution to the extensive magmatism are debated (cf., Pik et al., 1998; Kempton et al., 2000; Furman et al., 2006), and alternative models for LIP generation have been proposed (e.g.,

[1] We define as "fluid" a mobile phase which is not a carbonate or a silicate melt. Based on properties at the high P and T conditions of mantle rocks, fluids can have vapor-like, liquid-like, and transitional properties (cf., Manning, 2004; Keppler and Audétat, 2005)

.

Anderson, 2005; Foulger et al., 2005). The approach taken is a detailed study of H_2O bearing phases (fluid inclusions, amphibole, and nominally anhydrous minerals) in a suite of amphibole-bearing spinel lherzolites occurring at Injibara volcano, south-west of the Tana Lake (a summary of the petrography, and major element mineral chemistry has been presented by Ferrando et al., 2008). This volcanic centre is located on the Ethiopian plateau, at a marginal position with respect to the Afar and the Main Ethiopian Rift, i.e *foci* of continental breakup.

We will bring the first direct evidence of chlorine-rich H_2O-CO_2 metasomatic fluids preserved as inclusions in mantle minerals in the subcontinental lithosphere in a region of swelling and flood basalt formation. The Cl-rich, C-O-H composition of the metasomatic fluid phase, combined with calculated trace element patterns and H_2O-distribution in nominally anhydrous minerals, allow us to trace fluid-rock interaction involved in lithospheric enrichment processes, and to discuss fluid phase origin.

2. GEOLOGICAL FRAMEWORK

Ethiopia and Yemen have been affected by Oligocene to present flood basalt volcanism, prior to and concomitantly with the formation of the Ethiopian Rift Valley and the Afar depression (e.g., Mohr and Zanettin, 1988; Schilling and Kingsley, 1992; Deniel et al., 1994; Hofmann et al., 1997). The abundant basaltic volcanism, forming a wide continental flood basalt province, was accompanied by extensive regional uplift, and followed by rift opening and continental breakup (e.g., Mohr and Zanettin, 1988). It built up a thick succession of tholeiitic to Na-alkaline lavas and pyroclastic rocks, covering an area of about 600 km^2 (Fig. 1). Both the strong regional uplift preceding or accompanying the magmatic activity, and the spatial distribution of magma types have been interpreted by most Authors as evidence of emplacement of deep mantle plumes into the lithosphere, generating continental breakup and extensive magmatic activity (e.g., Schilling, 1973; Hofmann et al., 1997; Pik et al., 1998, 1999; Ebinger and Casey, 2001; Kieffer et al., 2004).

Various stages of volcanic activity are recognized. The basaltic plateau was formed during early stages, between about 50 to 10 Ma (e.g., Merla et al., 1979; Mohr and Zanettin, 1988), with eruption of flood tholeiitic to transitional basalts; these were accompanied by eruption of mildly alkaline trachytic and rhyolitic ignimbritic sheets, especially at the top of the basaltic sequence. The bulk of basaltic magmas was erupted in a rather short time interval, around 30 ± 1 m.y. (Zumbo et al., 1985; Baker et al., 1996; Hofmann et al., 1997; Ukstins et al., 2002). Successively,

several shield volcanoes of transitional to Na-alkaline basalts and minor trachytes were constructed (e.g. Piccirillo et al., 1979). Finally, Pliocene to Present volcanic activity took place mostly along the Main Ethiopian Rift and the Afar. Large variations in the petrological, geochemical and volcanological characteristics of the volcanism have been observed both in space and time in the Ethiopian-Afar-Red Sea volcanism (e.g., Deniel et al., 1994; Marty and Gezahegn, 1996; Pik et al., 1998, 1999; Chazot and Bertrand, 1993; Ayalew et al., 2002). These have been interpreted as related either to heterogeneities within an ascending deep mantle plume (Pik et al., 1999) and/or to interaction between deep plume material and the lithospheric mantle (Deniel et al., 1994) with an important role of crustal contribution (Pik et al., 1999; Ayalew et al., 2002).

Most petrological data on the subcontinental lithospheric Ethiopian mantle were obtained through the study of xenolith suites in Miocene-Quaternary alkali basalts from three different sections (Fig. 1): the Northern Ethiopian Plateau (Lake Tana region: Conticelli et al., 1999; Roger et al., 1999; Ferrando et al., 2008; Simien shield volcano: Ayalew et al., 2009), the Southern Main Ethiopian Rift (Mega; Bedini et al., 1997; Conticelli et al., 1999), and the Central Main Ethiopian Rift (Rooney et al., 2005). Beneath the Ethiopian plateau, Conticelli et al. (1999) and Roger et al. (1999) described an heterogeneous lithosphere, consisting of spinel-lherzolites with very subordinate harzburgites, dunites, and olivine websterites, which may locally contain amphibole. Recently, in Quaternary basanitic lavas from a cinder cone located 7-8 km SW of Injibara (Lake Tana region; Fig. 1), Ferrando et al. (2008) reported two suites of spinel-lherzolites: protogranular to porphyroclastic Cl-pargasite-bearing spinel lherzolites ($T \leq 1000°C$), which are also the subject of the present study; and granular spinel lherzolites (± amphibole), which underwent thermal recrystallization (1043 – 1167°C). Geochemical studies allowed to propose that the lithosphere beneath the Ethiopian plateau underwent two successive metasomatic events: modal metasomatism induced by a hydrous metasomatic agent, followed by cryptic metasomatism by alkali basaltic melts at higher temperatures.

3. ANALYTICAL TECHNIQUES

Major element analyses of minerals were carried out using a CAMECA SX50 electron microprobe at the IGAG, CNR in Roma. Operating conditions were 15 kV accelerating voltage, 15 nA beam current, and 10 s counting time for element. Natural and synthetic standards include: orthoclase (K), wollastonite (Ca, Si), native manganese (Mn), corundum (Al), jadeite (Na),

magnetite (Fe), native nickel (Ni), potassium chloride (Cl), periclase (Mg), native chromium (Cr), and rutile (Ti). At the operating conditions, values below 0.05 wt% for minor elements must be considered only indicative of very low contents (i.e. < 0.05 wt%). Structural formulae of minerals were processed using the software of Ulmer (1986). For amphiboles, the nomenclature of Leake et al. (2004) was followed.

In situ trace-element analysis of clinopyroxene and amphibole were performed on polished petrographic thin sections (100 µm thick) using the Laser Ablation – Inductively Coupled Plasma – Mass Spectrometer (LA-ICP-MS) installed at the University in Perugia (SMAArt facilities). The instrumentation consists of a New Wave UP213 frequency quintupled Nd:YAG laser ablation system coupled with a Thermo Electron X7 quadrupole based ICP-MS. All LA-ICP-MS measurements were carried out using time resolved analysis operating in a peak jumping mode. Each analysis consisted of ca. 40 s of measurement of instrumental background, i.e., analysis of the carrier gas with no laser ablation, followed by ca. 60-80 s of data acquisition with the laser on. The laser beam diameter, the repetition rate and the laser energy density were fixed to 30-40 µm, 10Hz and ~10J/cm^2, respectively. Helium was preferred over argon as a carrier gas to enhance transport efficiency of ablated aerosol (Eggins et al., 1998). The helium carrier exiting the ablation cell was mixed with argon make-up gas before entering the ICP torch to maintain stable and optimum excitation condition. External calibration was performed using NIST SRM 610 and 612 glass standards in conjunction with internal standardization using ^{42}Ca, previously determined by electron microprobe WDS following the method proposed by Longerich et al. (1996). Data reduction was performed using the Glitter software (van Achterbergh et al., 2001). The USGS reference material BCR2G (a fused glass of the Columbia River Basalt) was analyzed in each analytical run as quality control in order to assess the accuracy and the reproducibility of the analyses. Precision and accuracy for trace element determination are better than 10% in the standards. Further details on the analytical method can be found in Petrelli et al. (2007, 2008).

The composition of mineral phases within fluid inclusions was investigated with a Cambridge Instruments SEM Stereoscan 360 equipped with an EDS Energy 200 and a Pentafet detector (Oxford Instruments) at the University of Torino. Operating conditions were 15 kV accelerating voltage and 50 s counting time. SEM-EDS quantitative data (spot size = 2 µm) were acquired and processed using the Microanalysis Suite Issue 12, INCA Suite version 4.01; the raw data were calibrated on natural mineral standards and the ΦρZ correction (Pouchou and Pichoir, 1988) was applied.

Microthermometric measurements in fluid inclusions were done in eight samples with a Linkam THM 600 at the Siena University, calibrated using synthetic fluid-inclusion (SYNFLINC) temperature standards. In the temperature interval between -90 and 40 °C, the accuracy was estimated at 0.1°C at the standard reference points, and 0.2 °C at other temperatures. Isochores for inclusions are calculated using the ISOC computer program (Bakker, 2003).

Raman spectra were acquired with a Labram microprobe (HORIBA, Jobin-Yvon), equipped with a polarized 514.5-nm argon-ion laser at Siena University. The laser power was 300–500 mW at the source and about 80% less at the sample surface. The slit width was 100 µm, and the corresponding spectral resolution was ± 1.5 cm^{-1}. Raman spectra were collected through a 100× Olympus objective (excitation spot 1–2 µm in size) for an acquisition time of 30 or 60 s. Wavenumbers of the Raman lines were calibrated daily by the position of the diamond band at 1,332 cm^{-1}. The assignment of the Raman peaks was done by comparison with the reference database of mineral Raman spectra at the University of Siena (http://www.dst.unisi.it/geofluids/raman/spectrum_frame.htm), if not otherwise indicated. The analytical procedures applied for water detection in fluid inclusions are described in Frezzotti and Peccerillo (2007).

Fourier transform infrared (FTIR) microspectroscopy was performed at the infrared beam-line SISSI (Source for Imaging and Spectroscopic Studies in the Infrared) operating at the synchrotron laboratory ELETTRA in Trieste. Spectra were collected on a FTIR spectrometer (Bruker IFS66/v) fitted with an Hyperion IR microscopy with a liquid-nitrogen-cooled HgCdTe (MCT) detector. Infrared microscopy was performed on a infrared microscopy system (Bruker) with a x 16 magnification infrared objective. Spectra were collected at resolution of 4 cm^{-1} and signal averaged for 128 scans on each data collection. Background spectra were recorded in air. For IR imaging studies, we used double-polished thick sections of xenoliths of known thickness. The spectral images were collected scanning areas of variable sizes (200-400 µm-long and 200-400 µm-wide), following a regular grid of square-aperture dimension of 20 µm equidistant by 20 µm in both directions (i.e., totals of 100-400 spectra), using a computer-controlled automated X-Y mapping stage.

Interpretation of unpolarized spectra of H_2O followed the classical group frequency approach in which absorption bands are assigned to specific vibrational modes. OH concentrations in mineral phases were estimated from the integrated absorbance using the Beer-Lambert law (Paterson, 1982). Experimentally determined calibration constants for clinopyroxene and

orthopyroxene are from Bell et al. (1995), and for olivine are from Bell et al. (2003). Since unpolarized FTIR H_2O measurements are affected by large errors (30-50 %; cf., Demouchy et al., 2006), and imaging revealed H variations with position within single minerals, measuring the H_2O amounts with a precision at the ppm scale was complicated; thus, measured water contents are reported in intervals of tens of ppm, emphasizing the relative variations with distribution within single grains.

4. COMPOSITION OF PERIDOTITES

Deformed spinel lherzolites have protogranular to porphyroclastic textures (Fig. 2a) and contain two generations of olivine and orthopyroxene: large deformed porphyroclasts (2-4 mm), and polygonal neoblasts (up to 1 mm). Exsolution lamellae of clinopyroxene are usually present within porphyroclastic orthopyroxene (Fig. 2b). Clinopyroxene consists of smaller interstitial and tabular grains (≈ 1 mm), containing spinel exsolution lamellae (Fig. 2c). Brownish spinel has porphyroclastic or "holly-leaf" shape. Most deformed xenoliths contain weakly pleochroic amphibole (0.5 – 1 mm). Amphibole usually occurs in contact with clinopyroxene, and always contain relics of spinel, suggesting its grow from it (Fig. 2d).

Lherzolites have variable modal compositions with 50-69 olivine, 19-31 orthopyroxene, 9-20 clinopyroxene, 2-7 spinel, and amphibole ≤ 1, in vol.%. Comprehensive major element compositions of minerals have been reported in Ferrando et al. (2008). Olivine has Mg-numbers (mg# = $Mg/(Mg+Fe_{tot})*100$) from 89.2 to 89.6, lower than average cratonic mantle (Pearson et al., 2003). Spinel has mg# from 72.9 to 75.1, and cr# (cr# = Cr/Cr+Al*100) from 15 to 19 (Table 1). Both porphyroclasts and neoblasts of orthopyroxene are enstatite, with mg#= 89.9-90.3.

Clinopyroxene is a Ti-poor, Cr- Na-rich diopside (mg# = 89.8 – 91; Table 1). Clinopyroxene was analyzed for trace elements, illustrated in Fig. 3a and reported in Table 2. It shows LREE enrichment relative to HREE [La 10 -15 PM; $(La/Yb)_N = 4 – 2.5$] and flat REE patterns. HREE are relatively high, excluding re-equilibration with garnet, which would lead to much lower HREE contents. Remarkable features are the positive anomalies in LILE, particularly Th, U, and Pb, (Pb_N 20), and the LILE/HFSE fractionation (Pb_N/Nb_N = 10 - 50). Ti, Zr, and Hf show modest negative anomalies with respect to REE; Nb and Ta contents are lower than primordial mantle.

Amphibole is a Cr-rich pargasite, with mg# = 87.5-88.2 (Table 1). Although mantle amphibole is generally Cl-poor (typically < 0.05 wt %; e.g., Vannucci et al., 1995), pargasite has a

high Cl-content (0.33-0.37 wt%; Table 2). Pargasite has LREE [La 10 - 15 PM; $(La/Yb)_N \approx 4$], Pb, U, Th, and Sr enrichments quite similar to clinopyroxene (cf., Fig. 3 and Table 2), while tends to concentrate Ba (Fig. 3b). Although amphibole is the main host for Nb and Ta (e.g. Ionov and Hofmann, 1995), our pargasite does not show significant enrichments in these elements.

5. COMPOSITION AND DENSITY OF FLUID INCLUSIONS

Fluid inclusions are present in olivine and orthopyroxene porphyroclasts (Table 3; Fig. 4). Clinopyroxene generally does not contain fluid inclusions, with exception of a few grains (Fig. 4). Inclusions seem to have formed during a single fluid-rock interaction event; their distribution as small clusters and along trails, which never reach grain boundary edges, is indicative for early trapping (cf., Touret, 2001). Absence of inclusions in (olivine and orthopyroxene) neoblasts, in pargasite, and in most clinopyroxene grains, indicate formation just prior to or contemporaneously with recrystallization of peridotites. Glass (i.e., melt) has never been observed within fluid inclusions, and melt inclusions and/or glass on grain boundaries are absent in peridotites.

In orthopyroxene porhyroclasts, fluid inclusions consist of $CO_2 + H_2O$, or CO_2 ($CO_2 \geq 80$ vol. %; Fig. 4a and b). Liquid H_2O has been observed confined at the cavity borders only in a few large irregularly-shaped inclusions (Table 3). Water within inclusions was further identified by Raman analysis (Fig. 5a), and by microthermometric measurements (i.e., melting of clathrates, cf. Table 3). In olivine porphyroclasts only a few among the inclusions contain $CO_2 \pm H_2O$, while most inclusions appear to have reacted with the host olivine, and are filled by aggregates of phyllosilicates and a carbonate, without any noticeable fluid (step-daughter phases of Svensen et al., 1999; Table 3; Fig. 4c and d). Raman analyses identify the association of talc, or clinochlore + magnesite (Fig. 5b, c, and d). In clinopyroxene, rare fluid inclusions contain CO_2, but no H_2O or solids, and form short alignments along with abundant tiny amphibole inclusions (20 - 80 μm; arrows in Fig. 4e). Chemical analyses indicate these last ones as Cl-rich pargasite, identical to pargasite in the host rock (Table 1). The absence of H_2O in fluid inclusions does not indicate that the fluid was anhydrous: the association of Cl-pargasite + CO_2 inclusions testify for reaction of CO_2 - H_2O fluids with clinopyroxene to produce amphibole, leaving residual CO_2 trapped as inclusions.

CO_2 melting temperatures (Tm_{CO2}) were recorded between -57.6 and -56.2 °C (Table 3). Despite this large scattering of temperatures, only in a few inclusions Raman analyses detected traces of H_2S (< 0.1 mole %): the Tm's variation probably reflects thermal gradients within the

sample in the heating-cooling stage. A wide range of homogenization temperatures (Th) to the liquid phase was recorded between -39.2 and 31°C (Fig. 6). Water froze at temperatures of about -50°C, and first melting (Te) was recorded between -33 and -29°C (Table 3). Eutectic temperatures are indicative for the presence of metals (e.g. Mg^{2+} and Fe^{2+}) in addition to Na^{+} in the aqueous fluid, and freezing above the $CaCl_2$-NaCl-H_2O eutectic at -52°C suggests little or no Ca^{2+} in solution. In those inclusions containing both liquid and vapor CO_2, clathrate melting temperatures (Tm_{Clat}) correspond to salinities of 14 - 10 wt. % in NaCl eq. (Table 3).

The fluid composition was calculated as X_{CO2} = 0.64, X_{H2O} = 0.33 , X_{Na} = 0.006, X_{Mg} = 0.006, X_{Cl} = 0.018 (Bakker, 2003). In modeling fluid composition, Na^{+} and Mg^{2+} ions in the aqueous part of the fluid have been assumed present in subequal amounts, although the actual Mg/Na ratio of the fluid is not known. Such an assumption does not affect the bulk fluid density, and only slightly influences the Cl mole-fraction of the fluid. The resulting fluid density is 1.12 g/cm^3. At the inferred temperature of 950°C, based on mineral-mineral geothermometry (Ferrando et al., 2008), fluid isochores correspond to minimum pressures of mantle equilibration between 1.4 and 1.5 GPa, or 50 - 54 km (Holloway, 1981).

6. QUANTITATIVE H_2O MAPS IN NOMINALLY ANHYDROUS MINERALS

Chemical mapping of H_2O distribution was performed in olivine and orthopyroxene porphyroclasts and in clinopyroxene by synchrotron-sourced infrared microspectroscopy. The study focused on: i) quantification and distribution of H_2O stored in nominally anhydrous minerals; and ii) H_2O speciation and gradients between fluid inclusions and nominally anhydrous minerals.

In olivine not containing fluid inclusions, infrared absorption bands due to the stretching vibration of OH bond were recorded between 3450 and 3600 cm^{-1} (Fig. 7a and b). The wide majority of spectra (about 100 – 150) per single investigated area reflects disturbance by additional OH bands around 3680 cm^{-1}, which indicate the presence of talc and/or serpentine (Fig. 7c; Khisina et al., 2001; Matsyuk and Langer, 2004). Maps reveal that water is inhomogeneously distributed at the 20x20 µm scale: from 40 ± 20 ppm up to more than 120 ppm, due to the presence of hydrous phases (Fig. 7b). The image in Fig. 7c, reveals the distribution of talc/serpentine as 20 - 40 µm inclusions, and possibly as lamellae at the nanometric scale (cf. Khisina et al., 2001), since a general increase in the absorption intensities in the 3680 cm^{-1} region is observed through the analyzed area (yellow zone in Fig. 7c). In olivine containing fluid inclusions

exceedingly high water contents have been measured (200 - 440 ppm), which result from additional extrinsic OH absorption bands from molecular water in inclusions, and from the phyllosilicate formed by the reaction of the water contained within fluid inclusion and the host.

In inclusion-free clinopyroxene (Fig. 7d), water concentration ranges from 180 to 220 ppm, and increases noticeably upon approaching the grain boundary (600 - 800 ppm). Water enrichments are observed also within single crystals, where we document a an additional vibration of water close to at 3670 cm^{-1} (Fig. 7f), which is attributed to structurally bound OH in small nanometric pargasite inclusions (Hawthorne et al., 1997; Fig. 7e, and f). Rare clinopyroxene containing fluid inclusions (Fig. 7g) shows similar OH gradients, with hydroxyl-enriched rims (20 - 50 μm) as illustrated in Fig. 7h. Chemical imaging in the 3600 - 3800 cm^{-1} region further shows that hydration of clinopyroxene is coherent with the course of fluid inclusions (lower half of Fig. 7i). Those areas surrounding inclusions, spectra (lower half of Fig. 7h) contain an additional vibration at 3670 cm^{-1}, derived from extrinsic OH in pargasite inclusions (compare Fig. 7 h and i).

In orthopyroxene with no fluid inclusions, the chemical maps show a relatively homogeneous water distribution, with contents in the range of 80 - 100 ppm. In orthopyroxene containing fluid inclusions, a heterogeneous distribution of OH absorption intensities is observed, systematically higher in fluid inclusion rich areas. Here, as much as 450 ppm H_2O have been measured, due to additional absorption from extrinsic H_2O (molecular) contained in inclusions. Further, mapping revealed positive water gradients moving towards the fluid inclusions: from 80 ppm, at about a 100 μm from the fluid inclusion trail, progressively increasing close to areas containing inclusions (up to about 200 ppm; not shown). A similar gradient seem to indicate an effective transition from molecular water into OH-bond, resulting from loss from inclusions through dislocations and other defects (cf., Viti and Frezzotti, 2000).

7. DISCUSSION

7.1 The peridotites

Deformed spinel lherzolites represent a modally metasomatized lithosphere which underwent progressive recrystallization at relatively low temperatures (≤ 1000°C; Ferrando et al., 2008). Isochores calculated from fluid inclusion density data locate their depth of origin at 1.4 and 1.5 GPa, or 50-55 km (Holloway, 1981; Bakker, 2003). The petrography and mineral chemistry of

peridotites indicate that metasomatism resulted during a single event, either by crystallization from a melt or fluid phase, or by (melt-fluid)/solid reactions. Textural features, such as spinel being replaced by pargasite (e.g., Fig. 2d), and presence of pargasite inclusion trails in clinopyroxene (Fig. 4f) are indicative of (melt-fluid)/rock reactions.

Inferences on the composition of the metasomatic agents can be derived from the trace element composition of clinopyroxene and amphibole (Fig. 3). Clinopyroxene shows refertilization as evidenced by selective enrichments in most incompatible elements (LREE, Pb, Sr, U, Th), marked with depletion in HFSE. Amphibole mimics clinopyroxene trace element patterns, except for higher Ba, Rb, Nb, Ta, Ti and Cl (Fig. 3). Partition coefficients for trace elements are consistent with the clinopyroxene/amphibole relationships obtained from natural and experimental data (Ionov and Hofmann, 1995; Tiepolo et al., 2001), and suggest equilibrium behavior.

The observed trace elements enrichments are consistent with equilibration of lherzolites with an H_2O-rich metasomatic agent at high pressures: either an aqueous fluid, or a hydrous silicate melt probably evolved though porous flow (Bedini et al., 1997; Zanetti et al., 1999; Laurora et al., 2001; Ionov et al., 2002,; Rivalenti et al., 2004). Metasomatism mediated by carbonate-rich melts seems unlikely, firstly because of the absence of geochemical unequivocal markers, such as fractionation of Ti/Eu or Zr/Hf, and extreme LREE enrichment (up to 100 chondrite; Green and Wallace, 1988; Yaxley et al., 1991; Rudnick et al., 1992; Yaxley and Green 1996). Further, at the considered pressures, metasomatic carbonate melts would react with orthopyroxene to produce clinopyroxene, converting lherzolite into wehrlite (e.g., Yaxley et al.,1991; Rudnick et al.,1993). The investigated spinel lherzolites do not show any evidence for reaction of orthopyroxene, excluding a similar scenario.

Based on trace element distribution in metasomatic minerals only, however, it is difficult to discriminate between an aqueous fluid phase and a hydrous silica-rich melt as hypothetical metasomatic agents. The absence of a substantial U/Th fractionation is different from what would be expected from interaction with an aqueous fluid, but consistent with a silicate melt enriched in water (Stalder et al., 1998). Conversely, both the Cl-, and Ba-rich composition of amphibole, and the positive Pb/Sr correlation observed in amphibole and clinopyroxene suggests that the observed incompatible element increase was mediated via an aqueous fluid phase, since all these elements have high fluid/melt partition coefficients. The fractionation of Sr relative to Pb is also consistent with equilibration with an aqueous fluid: Pb behaves significantly more incompatibly than Srin H_2O fluids: Pb and Sr are incorporated at similar rate only through partial melting

processes in silicate melts, or in supercritical fluids at higher pressures (cf., Brenan et al., 1994, 1995; Kessel et al., 2005).

7.2. The metasomatic fluid phases

To assess the nature of the metasomatic agents involved in mantle enrichment processes in the Ethiopian lithospheric mantle, the chemical data from minerals are integrated with data from fluid inclusions. Fluid inclusions indicate that rocks have interacted with a Cl-rich H_2O-CO_2 fluid, i.e. metasomatism was fluid mediated. Further, the high Cl-content in pargasite, and the common association of fluid inclusions with pargasite inclusions in clinopyroxene suggests that Cl-rich fluids were contemporaneous and parental to pargasite growth.

Fluids contained within inclusions are dominated by CO_2 (≥ 64 mol.%). This corresponds to a_{H2O} of 0.2 of the fluid phase at the considered pressures. However, the original water content is underestimated, as infrared maps show H_2O diffusion from the inclusions to the host phase. The aqueous part of the fluid contain Cl, Na, and Mg - but not Ca - with salinities ranging between 10 and 14 % in NaCl + $MgCl_2$ eq. wt. (2 molal [NaCl - $MgCl_2$] solution). The Cl content is high, and calculated between 4 - 5 in mole %, depending on the Mg/Na ratio. Cl-rich fluids should also have contained SiO_2 and Al_2O_3, as suggested by formation of clinochlore and talc in inclusions reacting with olivine host (Pawley, 2003). At mantle conditions, high solubility of Si and Al is predicted, due to polymerization of these solutes in aqueous solutions, although the presence of CO_2 and NaCl tends to counteract this process (Newton and Manning, 2000).

Aqueous fluids involved in mantle enrichment processes at high pressure (1-2 GPa), especially concentrated solutions, have different properties than pure H_2O fluids; high Cl-contents (> 1 molal %) are known to strongly increase the solubility of metals (Mg, Fe, and Pb) and LILE (Keppler, 1996; Green and Adam, 2003; Manning, 2004). To better understand the possible effects of a high chlorine activity, trace element compositions of model fluids in equilibrium with clinopyroxene have been calculated, using experimental partition coefficients for clinopyroxene-H_2O ($D_{cpx\text{-}H2O}$), and for clinopyroxene-H_2O 5 molal NaCl ($D_{cpx\text{-}brine}$) (Keppler, 1996; Ayers, 1998); the results are shown in Fig. 8a. Calculated patterns for model brines (5 molal NaCl in Fig. 8a) in equilibrium with clinopyroxene show increasing higher incompatible element abundance, associated with prominent Pb and Sr positive anomalies and negative HFSE anomalies. Conversely, $D_{cpx\text{-}H2O}$, yields model pure H2O fluids with relatively unfractionated patterns, undepleted in HFSE,

and with significant enrichments only in Pb and U (H_2O in Fig. 8a). Model brines in equilibrium with clinopyroxene approach the composition of slab-derived brines (Fig. 8b; Scambelluri et al., 2002), and, to a lesser extent, that of carbonate-brine fluids in diamonds of eclogites (Fig. 8b; Tomlinson et al., 2009), but not that of carbonate-brine fluid in kimberlites (Fig. 8b; Tomlinson et al., 2009).

Thus, the metasomatic enrichment in the lithosphere beneath the Ethiopian plateau could have been induced by Cl-rich fluids preserved in fluid inclusions. Model trace-element composition appears to suggest similarities with patterns of slab-derived Cl-rich aqueous fluids. This last observation, however, should be taken cautiously, since geochemical inconsistencies with deep brines in diamonds could result from differences in fluid composition (i.e., presence of a carbonate component), and properties at different pressures.

7.3. Fluid distribution and content in the Ethiopian lithosphere

In the African lithospheric mantle, metasomatic growth of amphibole driven by hydrous ''fluids'' is observed in several localities and supposed to have occurred during the early stages of mantle upwelling. The amphibole-rich mantle under the Chyulu Hill Volcanic Province of southern Kenya is considered to have been modally metasomatized during early stages of the plume rising in the East African Rift (Späth et al., 2001). In a similar way, the growth of amphibole ± apatite in spinel peridotites from Yemen, is considered to have occurred during or shortly after the Oligocene by the influx of carbonatitic melts and hydrous fluids from the Afar plume (Baker et al., 1998). Besides, Cl-rich pargasite in spinel lherzolites of Zabargad Island (Red Sea) is interpreted to have grown just before the early rifting phase of the Red Sea (Agrinier et al., 1993). Metasomatism in spinel lherzolite suite demonstrates a major role for aqueous fluids also in the lithosphere beneath the Ethiopian plateau.

Minor pargasite in lherzolites is generally considered to be indicative of reaction of mantle rocks with minor amounts of hydrous fluids or melts. Present study argues for the presence of significant amounts of Cl-rich C-O-H- fluids in the Ethiopian lithosphere, which have a low water activity, resulting from presence of chlorine and other dilutants (e.g., CO_2). In addition to amphibole, water was stored into olivine and pyroxenes. Minimum calculated water contents within these nominally anhydrous minerals range around 40 ± 20 ppm for olivine, 100 ± 20 for orthopyroxene, and 220 ± 20 for clinopyroxene, corresponding to minimum water content of deformed lherzolites ≤ 150 ppm. These values are consistent with water contents measured in

423 nominally anhydrous minerals in spinel lherzolites (e.g., Ingrin and Skogby, 2000), and with
424 equilibrium partitioning of water between olivine and pyroxenes at the considered pressures
425 (Ingrin and Skogby, 2000; Bell and Rossman, 1992, Hauri et al., 2004).
426 Microinfrared maps of water distribution, however, identify zones of water enrichments at
427 the scale of the individual grain, generally not readily available, when measuring water with single
428 spot analyses: i) in most samples, olivine shows incipient hydration and locally stores up to 200 -
429 400 ppm H_2O (e.g. micro- to nano-inclusions of mg-phyllosilicates; Fig. 7b. ii). In clinopyroxene,
430 H_2O contents show a gradient, with extreme enrichments (up to 700 - 800 ppm) in the last 50 µm
431 at grain boundaries, and along intragranular bands in the internal parts (Fig. 7e, and h). Such a
432 zoning does not correspond to any other element (major or trace) zoning, with exception of a
433 slight La enrichment (Fig. 3); it could be considered suggestive of the presence of growth defects,
434 probably resulting from recrystallization in presence of aqueous fluids.
435 These observations lead to the conclusion that locally water amounts within deformed
436 spinel lherzolites could have been significantly higher and up to 400 - 500 ppm, without any
437 increase of the amount of amphibole in the rocks. Such an inhomogeneous water enrichment
438 through lherzolites has profound effects on the physical and chemical properties of lithospheric
439 mantle rocks: a heterogeneous distribution of those trace elements which are transported by
440 aqueous fluids, and a local overstep of C-O-H peridotite solidus, inducing partial melting, without
441 significant increases of temperatures.
442
443 **7.4. Significance of Cl-rich fluids in a region of asthenosphere upwelling and flood basalts.**
444
445 At Hawaii and Azores oceanic settings, Cl-enrichment in the lithosphere is indicated by the
446 high Cl/F ratios of melt inclusions in OIB, and interpreted to reflect shallow interaction with sea-
447 water or with deep-crustal brines (e.g., Michael and Schilling, 1989; Seaman et al., 2004; Stolper et
448 al., 2004; Le Roux et al., 2006). A similar explanation cannot apply to the continental lithospheric
449 mantle beneath the Ethiopian plateau. Here, metasomatism implies fluxes of C-O-H metasomatic
450 fluid phases rich in Cl and incompatible elements into the lithospheric mantle, likely related to
451 upwelling of the Afar mantle zone. Interactions between metasomatic fluids and mantle rocks
452 seem to have occurred heterogeneously, most likely by fracture migration, inducing selective
453 enrichments in volatiles and incompatible elements (LILE, and LREE) in the lithosphere. The source

454 of metasomatic fluids should have been located either in the upwelling asthenospheric mantle, or
455 in the lithosphere, where they started to migrate under the effect of increasing thermal anomalies.
456 Present data rise the question of Cl-enrichment in mantle fluids within the context of the
457 geodynamic evolution of the East African region. The high water and chlorine content (4-5 mole %)
458 of fluids suggests the presence of a cycled crustal (i.e., altered oceanic lithosphere) component in
459 their source. This is agreement with the extreme enrichments in Pb, Ba, Th, U, and Sr preserved in
460 amphibole and clinopyroxene, as generally assumed for sediments entrained in subducting
461 lithosphere (e.g. Ben Othman et al., 1989). Recycling of carbon has been shown in carbonatite
462 melts in oceanic peridotite xenoliths (e.g. Hauri et al., 1993) and can occur also for Cl, as Cl-rich
463 fluids found in eclogites and serpentinites can be recycled into the convecting mantle (cf., Pyle and
464 Mather, 2009, and references therein).
465 The upper mantle beneath Ethiopia was affected by ancient (Pan-African) subduction
466 processes. Therefore, it can be hypothesized that these elemental enrichments may be a remnant
467 of ancient subduction processes that were preserved in a fossilized lithospheric-asthenospheric
468 mantle, until the emplacement of hot mantle material generated their mobilization by
469 dehydration-decarbonation reactions, forming an ascending metasomatic Cl-rich CO_2-H_2O fluid
470 front. According to this hypothesis, the asthenospheric contribution to magmatism in the plateau
471 would be a function of both time (early magmatism more affected by lithosphere; Vidal et al.,
472 1991) and position with respect to Afar, which is the focus of extensional processes generated by
473 uprise of deep mantle material (Corti, 2009).
474 The preservation of textures, mineralogy, and fluid inclusions in a fossilized mantle for
475 hundreds of Ma after the Pan African orogeny is, however, enigmatic. An alternative scenario is
476 that CO_2 - brine fluids were derived by decarbonation and outgassing of deep hydro-saline
477 carbonate melts at pressures below 2 - 2.5 GPa. Presence of chlorine- and carbonate-rich fluid
478 phases at depth in the mantle would be consistent with the composition and metasomatic
479 signature of fluid phases preserved in diamonds at pressures above 4-5 GPa (Izraeli et al., 2001;
480 Klein-BenDavid et al., 2004; 2007; Tomlinson et al., 2009), and with melts in kimberlites
481 (Kamenetsky et al., 2004, 2007). Carbonate melts might have been generated by low degrees of
482 melting of a carbonated fertile peridotite, or of a carbonated and hydrated eclogite (Dalton and
483 Presnal 1988; Gudfinnsson and Presnall, 2005; Dasgupta and Hirschmann, 2006; Dasgupta et al.,
484 2007). Such melts have very low viscosities, and can rise through the upper mantle, degassing a
485 CO_2-H_2O-Cl fluid phase at pressures below the carbonate-stability field (2-2.5 GPa; Dobson et al.,

1996; Hammouda and Laporte, 2003). Noteworthy, fluxing of metasomatic CO_2 and H_2O from outgassing of hydrous carbonate melts has been recently proposed in the lithosphere beneath Hawaii, based on the association of CO_2-H_2O fluids, carbonates, and diamonds preserved in fluid inclusions of garnet pyroxenite xenoliths (Frezzotti and Peccerillo, 2007).

8. Summary

In conclusion, present data provide the first direct evidence for Cl-rich CO_2-H_2O fluids fluxing the lithosphere of a region of continental flood basalts. Despite the uncertainties in the fluid recycling record, the chemical and physical properties of Cl-rich fluids suggest an origin in the upper mantle, probably at pressure above 2.5 GPa. Volatile enrichment and refertilization in the lithosphere beneath the Ethiopian plateau induced by Cl-rich fluids might have played a key role in facilitating melting, such that magmatism could have been generated without a significant increase of mantle temperatures. Further, elemental enrichment by similar fluids may provide an explanation for the geochemical trace element signature of some LIP magmas (i.e., strong positive spikes of Ba and Pb). Finally, our findings complement ongoing fluid inclusion research in diamonds and kimberlites (e.g., Izraeli et al., 2001; Kamenetsky et al., 2004; 2007; Klein-BenDavid et al., 2004; 2007; Tomlinson et al., 2009) and highlight the important role of Cl in aqueous fluids at mantle depth.

ACNOWLEDGEMENTS

We are grateful for the constructive reviews from M. A. Menzies and three anonymous reviewers. We are indebted to M. Serracino for assistance during microprobe analyses. This work was funded by national (MIUR 2008) funds to M.L.F. and A.P.. Raman analyses facilities were provided by PNRA, the national research group for Antarctica. Access to the Synchrotron in Trieste was funded by Elettra and the EU.

514 **REFERENCES**

515 Agrinier P., Mével C., Bosch D., and Javoy M. (1993) Metasomatic hydrous fluids in amphibole
516 peridotites from Zabargad Island (Red Sea). *Earth Planet. Sci. Lett.* **120**, 187-205.
517 Andersen T. and Neumann E. R. (2001) Fluid inclusions in mantle xenoliths. *Lithos* **55**, 301-320.
518 Anderson D. L. (2005) Large igneous provinces, delamination, and fertile mantle. *Elements* **1**, 271-
519 275.
520 Ayalew D., Barbey P., Marty B., Reisberg L., Yirgu G. and Pik R. (2002) Source, genesis, and timing
521 of giant ignimbrite deposits associated with Ethiopian continental flood basalts. *Geochim.*
522 *Cosmochim. Acta* **66**, 1429-1448.
523 Ayalew D., Arndt N., Bastien F., Yirgu G., and Kiefer B. (2009) A new mantle xenolith locality from
524 Simien shield volcano, NW Ethiopia. *Geol. Mag.* **146** , 144-149.
525 Ayers J. (1998) Trace element modeling of aqueous fluid– peridotite interaction in the mantle
526 wedge of subduction zones. *Contrib. Mineral. Petrol.* **132**, 390-404.
527 Baker J. A. , Snee L. and Menzies M. (1996) A brief Oligocene period of flood volcanism in Yemen:
528 implications for the duration and rate of continental flood volcanism at the Afro-Arabian
529 triple junction. *Earth Planet. Sci. Lett.* **138**, 39-55.
530 Baker J. A., Chazot C., Menzies M., and Thirwall M. (1998) Metasomatism of the shallow mantle
531 beneath Yemen by the Afar plume: Implications for plumes, flood volcanism, and intraplate
532 volcanism. *Geology* **26**, 431-434.
533 Bakker R. J. (2003) Package FLUIDS 1. New computer programs for the analysis of fluid inclusion
534 data and for modelling bulk fluid properties. *Chem. Geol.* **194**, 3-23.
535 Bedini R. M., Bodinier J. L., Dautria J. M. and Morten L. (1997) Evolution of LILE-enriched small
536 melt fractions in the lithospheric mantle: a case study from the East African Rift. *Earth Planet.*
537 *Sci. Lett.* **153**, 67-83.
538 Bell D. R. and Rossman G. R. (1992) Water in Earth's mantle: The role of nominally anhydrous
539 minerals. *Science* **255**, 1391-1397.
540 Bell D. R., Ihinger P. D., and Rossman G. R. (1995) Quantitative analysis of trace OH in garnet and
541 pyroxenes. *Am. Mineral.* **80**, 465-474.
542 Bell D. R., Rossman G. R., Maldener J., Endisch D., and Rauch F. (2003) Hydroxide in olivine: a
543 quantitative determination of the absolute amount and calibration of the IR spectrum. *J.*
544 *Geophys. Res.* **108**, 2105. doi:10.1029/2001JB000679
545 Ben Othman D., White W. M., and Patchett J. (1989) The geochemistry of marine sediments, island
546 arc magma genesis, and crustal-mantle recycling. *Earth Planet. Sci. Lett.* **94**, 1-21.
547 Brenan J. M., Shaw H. F., Phinney D. L., and Ryerson F. J. (1994) Rutile-aqueous fluid partitioning of
548 Nb, Ta, Hf, Zr, U and Th: implications for high field strength element depletions in island-arc
549 basalts. *Earth Planet. Sci. Lett.* **128**, 327-339.
550 Brenan J. M., Shaw H. F., Ryerson F. J., and Phinney D. L. (1995) Mineral-aqueous fluid partitioning
551 of trace elements at 900°C and 2.0 GPa: Constraints on the trace chemistry of mantle and
552 deep crustal fluids. *Geochim. Cosmochim. Acta* **59**, 3331-3350.
553 Chazot G. and Bertrand H. (1993) Mantle sources and magma-continental crust interactions during
554 early Red Sea-Aden rifting in Southern Yemen: Elemental and Sr, Nd, Pb isotope evidence. *J.*
555 *Geophys. Res.* **98**, 1818-1835.
556 Condie K.C. (2001) Mantle Plumes and Their Records in Earth History, pp. 306. Cambridge
557 University Press, New York.
558 Corti G. (2009) Continental rift evolution: From rift initiation to incipient break-up in the Main
559 Ethiopian Rift, East Africa. *Earth Sci. Rev.* **96**, 1-53.

Conticelli S., Sintoni M. F., Abebe T., Mazzarini F., and Manetti P. (1999) Petrology and geochemistry of ultramafic xenoliths and host lavas from the Ethiopian Volcanic Province: an insight into the upper mantle under Eastern Africa. Acta Vulcanol. 11, 143-159.

Dalton J. A. and Presnall D. C. (1998) The continuum of primary carbonatitic–kimberlitic melt compositions in equilibrium with lherzolite: Data from the system CaO-MgO-Al_2O_3-SiO_2-CO_2 at 6 GPa. *J. Petrol.* **39**, 1953-1964.

Dasgupta R. and Hirschmann M. M. (2006) Melting in the Earth's deep upper mantle caused by carbon dioxide. *Nature* **440**, 659-662.

Dasgupta R., Hirschmann M. M., and Smith N. D. (2007). Partial melting experiments of peridotite + CO2 at 3 GPa and genesis of alkalic ocean island basalts. *J. Petrol.* **48**, 2093-2124.

Demouchy S., Jacobsen S. D., Gaillard F., and Stern C. R. (2006) Rapid magma ascent recorded by water diffusion profiles in mantle olivine. *Geology* **34**, 429-432.

Deniel C., Vidal P., Coulon C., Vellutini P. J., and Piguet P. (1994) Temporal evolution of mantle sources through continental rifting: The volcanism of Djibouti (Afar). *J. Geophys. Res.* **99**, 2853-2869.

Dobson, D.P., Jones A.P., Rabe R., Sekine T., Kurita K., Taniguchi T., Kondo T., Kato T., Shimomura O., and Urakawa S. (1996) In-situ measurement of viscosity and density of carbonate melts at high pressure. *Earth Planet. Sci. Lett.* **143**, 207-215.

Ebinger C. J. and Casey M. (2001) Continental breakup in magmatic provinces: An Ethiopian example. *Geology* **29,** 527-530.

Eggins S.M., Kinsley L. P. J., and Shelley J. M. G. (1998) Deposition and fractionation processes during atmospheric pressure laser sampling for analysis by ICP-MS. *Appl. Surf. Sci.* **129**, 278.

Ernst R. E. Buchan K. L. (2003) Recognizing mantle plumes in the geological record. *Annual Rev. Earth Planet. Sci.* **31**, 469-523.

Falloon T. J. and Green D. H. (1989) The solidus of carbonated, fertile peridotite. *Earth Planet. Sci. Lett.* **94**, 364-370.

Ferrando S., Frezzotti M. L., Neumann E. R., De Astis G., Peccerillo A., Dereje A., Gezahegn Y., and Teklewold A. (2008) Composition and thermal structure of the lithosphere beneath the Ethiopian plateau: evidence from mantle xenoliths in basanites, Injibara, Lake Tana Province. *Mineral. Petrol.* **93**, 47-78.

Foulger G. R., Natland J. H., Presnall D. C., and Anderson D. L. (Eds.) (2005) Plates, Plumes and Paradigms, pp. 881. Special Publication **388**. Geological Society of America.

Frezzotti M. L. and Peccerillo A. (2007) Diamond-bearing COHS fluids in the mantle beneath Hawaii. *Earth Planet. Sci. Lett.* **262**, 273-283.

Frezzotti M. L., Andersen T., Neumann E. R, and Simonsen S. L. (2002a) Carbonatite melt-CO_2 fluid inclusions in mantle xenoliths from Tenerife, Canary Islands: a story of trapping, immiscibility and fluid–rock interaction in the upper mantle. *Lithos* **64**, 77-96.

Frezzotti M. L., Neumann E. R., and Touret J. L. R. (2002b) Ephemeral carbonate melts in the upper mantle: carbonate-silicate immiscibility in microveins and inclusions within spinel peridotite xenoliths, La Gomera, Canary Islands. *Eur. J. Mineral.* **14**, 5, 891-904.

Frost R., Palmer S., Bouzaid J. and Reddy J. (2007) A Raman spectroscopic study of humite minerals. *J. Raman Spectr.* **38**, 68-77.

Furman T., Bryce J., Rooney T., Hanan B., Yirgu G., and Ayalew D. (2006) Heads or tails: 30 million years of the Afar plume. In *The structure and Evoltution of the east African rift system in the Afar volcanic province* (eds. G. Yirgu, C. J. Ebinger, and P.K.H. Maguire) pp. 97-121. Special Publication **259.** Geological Society of London.

Green D. H. and Wallace M. E. (1988) Mantle metasomatism by ephemeral carbonatite melts. *Nature* **336**, 459-462.

608 Green D. H. and Falloon T. J. (1998) Pyrolite: a Ringwood concept and its current expression. In *The*
609 *Earth's Mantle* (ed. J. Jackson), Cambridge Univ. Press, New York, pp. 311-378.
610 Green T. H. and Adam J. (2003) Experimentally-determined trace element characteristics of
611 aqueous fluid from partially dehydrated mafic oceanic crust at 3.0 GPa, 650-700°C. *Eur. J.*
612 *Mineral.* **15**, 815-830.
613 Gudfinnsson G.H. and Presnall D.C. (2005) Continuous gradations among primary carbonatitic,
614 kimberlitic, melilititic, basaltic, picritic, and komatiitic melts in equilibrium with garnet
615 lherzolite at 3-8 GPa. *J. Petrol.* **46**, 1645-1659.
616 Hammouda T. and Laporte D. (2000) Ultrafast mantle impregnation by carbonatite melts. *Geology*
617 **28**, 283-285.
618 Hauri E.H., Shimizu N., Dieu, J.J., and Hart S.R. (1993) Evidencef or hotspot-related carbonatite
619 metasomatism in the oceanic upper m antle. *Nature* **365**, 221-227.
620 Hauri E. H., Gaetani G., and Green T. H. (2004) Partitioning of H_2O between mantle minerals and
621 silicate melts, *Geochim. Cosmochim. Acta* **68**, A33 (abstr.).
622 Hawthorne F. C., Della Ventura G., Robert J.-L., Welch M. D., Raudsepp M., and Jenkins D. M.
623 (1997) A Rietveld and infrared study of synthetic amphiboles along the potassium-richterite–
624 tremolite join. *Am. Mineral.* **82**, 708-716.
625 Hofmann C., Courtillot G., Feraud G., Rochette P., Yirgu G., Ketefo E., and Pik R. (1997) Timing of
626 the Ethiopian flood basalt event and implication for plume birth and global change. *Nature*
627 **389**, 838-841.
628 Holloway J.R. (1981) Compositions and volumes of supercritical fluids in the earth's crust. In *Short*
629 *course in fluid inclusions: Applications to petrology* (eds. L.S. Hollister and M.L. Crawford)
630 Mineral. Ass. Canada, Calgary, pp. 13-38.
631 Ingrin J. and Skogby H. (2000) Hydrogen in nominally anhydrous upper-mantle minerals:
632 Concentration levels and implications. *Eur. J. Mineral.* **12**, 543-570.
633 Ionov D. A. and Hofmann A. W. (1995) Nb-Ta-rich mantle amphiboles and micas: implications for
634 subduction-related metasomatic trace element fractionations. *Earth Planet. Sci. Lett.* **131**,
635 341-356.
636 Ionov D. A., Bodinier J.-L., Mukasa S. B., and Zanetti A. (2002) Mechanisms and sources of mantle
637 metasomatism: major and trace element compositions of peridotite xenoliths from
638 Spitsbergen in the context of numerical modeling. *J. Petrol.* **43**, 2219-2259.
639 Izraeli E. S., Harris J. W., and Navon O. (2001) Brine inclusions in diamonds: a new upper mantle
640 fluid. *Earth Planet. Sci. Lett.* **187**, 323-332.
641 Kamenetsky M.B., Sobolev A.V., Kamenetsky V.S., Maas R., Danyushevsky L.V., Thomas R.,
642 Pokhilenko N.P., Sobolev N.V. (2004). Kimberlite melts rich in alkali chlorides and
643 carbonates: a potent metasomatic agent in the mantle. *Geology* **32**, 845–848.
644 Kamenetsky V.S., Kamenetsky M.B., Sharygin V.V., Faure K., Golovin A.V. (2007) Chloride and
645 carbonate immiscible liquids at the closure of the kimberlite magma evolution (Udachnaya-
646 East kimberlite, Siberia). *Chem. Geol.* **237**, 384–400.
647 Kempton P.D., Fitton J.G., Saunders A.D., Nowell G.M., Taylor R.N., Hardarson B.S., and Pearson G.
648 (2000) The Iceland plume in space and time. *Earth Planet. Sci. Lett.* **177**, 255-271.
649 Keppler H. (1996) Constraints from partitioning experiments on the composition of subduction-
650 zone fluids. *Nature* **380**, 237-240.
651 Keppler H. and Audétat A. (2005) Fluid-mineral interaction at high pressures. In *Mineral behavior*
652 *at extreme conditions* (ed. R. Miletich), Eur. Mineral. Union, Lecture notes in Mineral. **7**. pp.
653 1-30.
654 Kessel R., Schmidt M. W., Ulmer P., and Pettke T. (2005) Trace element signature of subduction-
655 zone fluids, melts and supercritical liquids at 120-180 km depth. *Nature* **437**, 724-727.

Khisina N. R., Wirth R., Andrut M., and Ukhanov A.V. (2001) Extrinsic and intrinsic mode of hydrogen occurrence in natural olivines: FTIR and TEM investigation. *Phys. Chem. Miner.* **28**, 291-301.

Kieffer B., Arndt N., Lapierre H., Bastien F., Bosch D., Pecher A., Yirgu G., Ayalew D., Weis D., Jerram D. A., Keller F., and Meugniot C. (2004) Flood and shield basalts from Ethiopia: magmas from the African Superswell. *J. Petrol.* **45**, 793-834.

Klein-BenDavid O., Izraeli E. S., Hauri E., and Navon O. (2004) Mantle fluid evolution—a tale of one diamond. *Lithos* **77**, 243-253.

Klein-BenDavid O., Izraeli E. S., Hauri E., and Navon O. (2007) Fluid inclusions in diamonds from the Diavik mine, Canada and the evolution of diamond-forming fluids. *Geochim. Cosmochim. Acta* **71**, 723-744.

Kleppe A. K., Jephcoat A. P., and Welch M. D. (2003) The effect of pressure upon hydrogen bonding in chlorite: A Raman spectroscopic study of clinochlore to 26.5 GPa. *Am. Mineral.* **88**, 567-573.

Laurora A., Mazzucchelli M., Rivalenti G., Vannucci R., Zanetti A., Barbieri M. A., and Cingolani C. A. (2001) Metasomatism and Melting in Carbonated Peridotite Xenoliths from the Mantle Wedge: The Gobernador Gregores Case (Southern Patagonia). *J. Petrol.* **42**, 69-87.

Le Roux P. J., Shirey S. B., Hauri E. H., Perfit M. R., and Bender J. F. (2006) The effects of variable sources, processes and contaminants on the composition of northern EPR MORB (8-108N and 12-148N): Evidence from volatiles (H_2O, CO_2, S) and halogens (F, Cl). *Earth Planet. Sci. Lett.* **251**, 209-231.

Leake B. E., Woolley A. R., Birch W. D., Burke E. A. J., Ferraris G., Grice J. D., Hawthorne F. C., Kisch H. J., Krivovichev V. G., Schumacher J. C., Stephenson N. C. N., and Whittaker E. J. W. (2004) Nomenclature of amphiboles: additions and revisions to the International Mineralogical Association's amphibole nomenclature. *Eur. J. Mineral.* **16**, 191-196.

Longerich H. P., Jackson S. E., and Günter D. (1996) Laser ablation-inductively coupled plasma mass spectrometric transient signal data acquisition and analyte concentration calculation. *J. Anal. Atomic Spectrom.* **11**, 899-904.

Manning C. E. (2004) The chemistry of subduction-zone fluids. *Earth Planet. Sci. Lett.* **223**, 1-16.

Marty B., Pik R., and Gezahegn Y. (1996) Helium isotopic variations in Ethiopian plume lavas: Nature of magmatic sources and limit on lower mantle contribution. *Earth Planet. Sci. Lett.* **144**, 223-237.

Matsyuk S. S. and Langer K. (2004) Hydroxyl in olivines from mantle xenoliths in kimberlites of the Siberian Platform. *Contrib. Mineral. Petrol.* **147**, 413-437.

McDonough W. F. and Sun S. S. (1995) Composition of the earth. *Chem. Geol.* **120**, 223-253.

Merla G., Abbate E., Canuti P., Sagri M., and Tacconi P. (1979) Geological map of Ethiopia and Somalia and comment, pp. 89. Consiglio Nazionale delle Ricerche, Firenze.

Michael, P. J. and Schilling J.-G. (1989) Chlorine in mid-ocean ridge magmas: evidence for assimilation of seawater-influenced components. *Geochem. Cosmochim. Acta* **53**, 3131-3143.

Mohr P. and Zanettin B. (1988) The Ethiopian flood basalt province. In *Continental Flood Basalts* (ed. J. D. Macdougall), pp. 63-110. Kluwer Academic Publishing.

Navon O., Hutcheon I. D., Rossman G. R., and Wasserburg G. J. (1988) Mantle-derived fluids in diamond micro-inclusions. *Nature* **335**, 784-789.

Newton R.C. and Manning C.E. (2000) Quartz solubility in concentrated aqueous NaCl solutions at deep crust– upper mantle metamorphic conditions: 2-15 kbar and 500-900 °C. *Geochim. Cosmochim. Acta* **64**, 2993– 3005.

Paterson M. (1982) The determination of hydroxyl by infrared absorption in quartz, silicate glasses and similar materials: *Bull. Minéral.* **105**, 20-29.

Pawley A. (2003) Chlorite stability in mantle peridotite: the reaction clinochlore + enstatite = forsterite + pyrope + H_2O. *Contrib. Mineral. Petrol.* **144**, 449-456.

Petrelli M., Perugini D., Poli G., and Peccerillo A. (2007) Graphite electrode tetraborate fusion for automated trace element determination in bulk samples by laser ablation ICP-MS. *Microchim. Acta* **158**, 275-282.

Petrelli M., Perugini D., Alagna K. E., Poli G., and Peccerillo A. (2008) Spatially Resolved and Bulk Trace Element Analysis by Laser Ablation - Inductively Coupled Plasma - Mass Spectrometry (LA-ICP-MS). *Per. Mineral.* **77**, 3-21.

Piccirillo E. M., Justin-Visentin E., Zanettin B., Joron J. K., and Treuil M. (1979) Geodynamic evolution from plateau to rift: Major and trace element geochemistry of the central eastern Ethiopian plateau volcanics. *Neues Jahr. Geol. Palaont.* **258**, 139-179.

Pik R., Deniel C., Coulon C., Yirgu G., Hofmann C., and Ayalew D. (1998) The Northwestern Ethiopian plateau flood basalts: Classification and spatial distribution of magma types. *J. Volcanol. Geotherm. Res.* **81**, 91-111.

Pik R., Deniel C., Coulon C., Yirgu G., and Marty B. (1999) Isotopic and trace element signatures of Ethiopian flood basalts: Evidence for plume-lithosphere interaction. *Geochim. Cosmochim. Acta* **63**, 2263-2279.

Pouchou J. L. and Pichoir F. (1988) Determination of mass absorption coefficients for soft X-Rays by use of the electron microprobe. In *Microbeam Analysis*, pp. 319–324. San Francisco Press.

Pyle D. M. and Mather T. A. (2009) Halogens in igneous systems. *Chem. Geol.* **263**, 110-121.

Rivalenti G., Mazzucchelli M., Laurora A., Ciuffi S. I. A. , Zanetti A., Vannucci R., and Cingolani C. A. (2004) The backarc mantle lithosphere in Patagonia, South America. *J. South Am. Earth Sci.* **17**, 121-152.

Roedder E. (1965) Liquid CO_2 inclusions in olivine-bearing nodules and phenocrysts from basalts *Am. Mineral.* **50**, 1746-1782.

Roger S., Dautria J. M., Coulon C., Pik R., Yirgu G., Michard A., Legros P., and Ayalew D. (1999) An insight on the nature, composition and evolution of the lithospheric mantle beneath in the north-western Ethiopian plateau: the ultrabasic xenoliths from the Tana Lake Province. *Acta Vulcanol.* **11**, 161-168.

Rooney T. O., Furman T., Yirgu G., and Ayalew D. (2005) Structure of the Ethiopian lithosphere: xenolith evidence in the Main Ethiopian Rift. *Geochim. Cosmochim. Acta* **69**, 3889-3910.

Rudnick R. L., McDonough W. F., and Orpin A. (1992) Tanzanian peridotite xenoliths: a comparison with Kaapvaal peridotites and inferences on metasomatic interactions. In *Kimberlites, related rocks and mantle xenoliths*. Vol. 1. (eds. H. O. A. Meyer and O. Leonardos) pp. 336-353. Proc. 5^{th} Inter. Kimberlite Conf., CPRM, Brasilia.

Rudnick R. L., McDonough W. F., and Chappell B. W. (1993) Carbonatite metasomatism in the Northern Tanzanian mantle - petrographic and geochemical characteristics. *Earth Planet. Sci. Lett.* **114**, 463-475.

Scambelluri M., Bottazzi P., Trommsdorff V., Vannucci R., Hermann J., Gomez-Pugnaire M.T., Lopez-Sanchez Vizcaıno V. (2002) Incompatible element-rich fluids released by antigorite breakdown in deeply subducted mantle, *Earth Planet. Sci. Lett.*, **192**, 457–470.

Schiano P., Clocchiatti R., Shimizu N., Maury R. C., Jochum K. P., and Hoffman A.W. (1995) Hydrous silica-rich melts in the sub-arc mantle and their relationship with erupted arc lavas. *Nature* **377**, 595-600.

Schilling J. G. (1973) Afar mantle plume: Rare earth evidence. *Nature* **242**, 2-5.

Schilling J.G. and Kingsley R.H. (1992) Nd–Sr–Pb isotopic variations along the Gulf of Aden: evidence for Afar Mantle Plume – Continental Lithosphere interaction. *J Geophys. Res.* **97** (B7): 10927–10966

Seaman C., Sherman S. B., Garcia M. O., Baker M. B., Balta B., and Stolper E. (2004) Volatiles in glasses from the HSDP2 drill core. *Geochem. Geophys. Geosyst.* ***5***, Q09G16 doi: 10.1029/2003GC000596

Späth A., Le Roex A. P., and Opiyo-Akech N. (2001) Plume-lithosphere interaction and the origin of continental rift-related alkali volcanism-the Chyulu Hills volcanic province, southern Kenya. *J. Petrol.* ***42***, 765-787.

Stalder R., Foley S. F., Brey G. P., and Horn I. (1998) Mineral-aqueous fluid partitioning of trace elements at 900-1200°C and 3.0-5.7 GPa: new experimental data for garnet, clinopyroxene, and rutile, and implications for mantle metasomatism - evidence from high-pressure experiments and natural rocks. *Geochim. Cosmoch. Acta* **62**, 1781-1801.

Stolper E., Sherman S., Garcia M. O., Baker M. B., and Seaman C. (2003) Glass in the submarine section of the HSDP2 drill core, Hilo, Hawaii. *Geochem. Geophys. Geosyst.* **5**, Q07G15, doi: 10.1029/2003GC000553.

Svensen H., Jamtveit B., Yardley B. W., Eengvik A. K., Austrheim H. and Broman C. (1999) Lead and Bromine enrichment in eclogite facies fluids: extreme fractionation during lower crustal hydration. *Geology* **27**, 467-470.

Thompson A. B. (1992) Water in the Earth's Upper Mantle. *Nature* **358**, 295-302.

Tiepolo M., Bottazzi P., Foley S., Oberti R., Vannucci R., and Zanetti A. (2001) Fractionation of Nb and Ta from Zr and Hf at mantle depths: the role of titanian pargasite and kaersutite. *J. Petrol.* **42**, 221-232.

Tomlinson E.L., Müller W. and EIMF (2009) A snapshot of mantle metasomatism: Trace element analysis of coexisting fluid (LA-ICP-MS) and silicate (SIMS) inclusions in fibrous diamonds. *Earth Planet. Sci. Lett.* **279**, 362-372.

Touret J.L.R. (2001) Fluids in metamorphic rocks. In *Fluid inclusions: Phase relationships – methods – applications*. (eds. T. Andersen, M.L. Frezzotti, E. Burke), pp. 1-27. Lithos **55**.

Ukstins I., Rennes P., Wolfenden E., Baker J., Ayalew D., and Menzies M. (2002) Matching conjugate volcanic rifted margins: $^{40}Ar/^{39}Ar$ chronostratigraphy of pre- and syn-rift bimodal flood volcanism in Ethiopia and Yemen. *Earth Planet. Sci. Lett.* **198**, 289-306.

Ulmer P. (1986) NORM-Program for cation and oxygen mineral norms. Computer Library, Institut fûr Mineralogie und Petrographie, ETH-Zentrum, Zürich, Switzerland.

van Achterbergh E., Ryan C. G., Jackson S., and Griffin W. L. (2001) Data reduction software for LA-ICP-MS. In *Laser-Ablation-ICPMS in the earth sciences, principles and applications* (ed. P. Sylvester), pp. 239-243. Short Course Series **29**. Mineralogical Association Canada.

Vannucci R., Piccardo G. B., Rivalenti G., Zanetti A., Rampone E., Ottolini L., Oberti R., Mazzucchelli M., and Bottazzi P. (1995) Origin of LREE-depleted amphiboles in the subcontinental mantle. *Geochim. Cosmochim. Acta* **59**, 1763-1771

Vidal P. H., Deniel C., Vellutini P. J., Piguet P., Coulon C., Vincent J., and Audin J. (1991) Changes of mantle sources in the course of a rift evolution: The Afar case. *Geophys. Res. Lett.* **18**, 1913-1916.

Viti C. and Frezzotti M.L. (2000) Re-equilibration of glass and CO2 inclusions in xenolith olivine: a TEM study. *Am. Mineral.* **85**, 1390-1396.

Wallace M. E. and Green D. H. (1988) An experimental-determination of primary carbonatite magma composition. *Nature* **335**, 343-346.

White R. S. and McKenzie D. (1995) Mantle plume and flood basalts. *J. Geophys. Res*. **100**, 17543-17585.

Wyllie P. J. and Ryabchikov I. D. (2000) Volatile components, magmas, and critical fluids in upwelling mantle. *J. Petrol.* **41**, 1195-1206.

Yaxley G. M., Crawford A. J., and Green, D. H. (1991) Evidence for alkaline glasses and carbonatite metasomatism in spinel peridotite xenoliths from western Victoria, Australia. *Earth Planet. Sci. Lett.* **107**, 305–317.

Yaxley G. M. and Green D. H. (1996) Experimental reconstruction of sodic dolomitic carbonatite melts from metasomatised lithosphere. *Contrib. Mineral. Petrol.* **124**, 359-369.

Zanetti A., Mazzucchelli M., Rivalenti G., and Vannucci R. (1999) The Finero phlogopite-peridotite massif: an example of subduction-related metasomatism. *Contrib. Mineral. Petrol.* **134**, 107-122.

Zumbo V., Feraud G., Betrand H., and Chazot G (1995) $^{40}Ar/^{39}Ar$ chronology of Tertiary magmatic activity in southern Yemen during the early Red Sea-Aden rifting. *J. Volcanol. Geother. Res.* **65**, 265-279.

812 **Figure captions**
813

814 Fig. 1. Simplified geological sketch map of Ethiopia, reporting sampling locality (black star)
815 modified from Conticelli et al., 1999, Roger et al., 1999, and Kieffer et al., 2004. MER: Main
816 Ethiopian Rift; EVP: Ethiopian Volcanic Plateau.
817 Fig. 2. Photomicrographs of spinel lherzolites from Injibara. a) Deformed lherzolite showing
818 porphyroclastic texture. Sample INJ35, crossed polars (CP). b) Porphyroclast of orthopyroxene
819 showing exsolution lamellae of clinopyroxene. Sample INJ16, plane-polarized light (PPL). c)
820 Clinopyroxene in textural equilibrium with porphyroclastic olivine. Spinel segregations are
821 evident within clinopyroxene. Sample INJ16, PPL. d) Relict ''holly-leaf'' Spl partly replaced by
822 brown-to-yellow amphibole. A very fine-grained corona grows on it. Sample INJ35, PPL. Ol I =
823 olivine porphyroclast; Ol II = olivine neoblast; Opx II orthopyroxene neoblast; Cpx =
824 clinopyroxene; Spl = spinel.
825 Fig. 3. Trace element concentrations (a) in clinopyroxene (Cpx) core and rim, and (b) in amphibole,
826 normalized to primordial mantle (PM) using the data from McDonough and Sun (1995). Data
827 below detection limits that connected with dashed lines and plotted as detection limit values.
828 Fig. 4. Photomicrographs of fluid inclusions in spinel lherzolites. a) Fluid inclusion distribution
829 along microfractures in orthopyroxene. A few large inclusions (arrow) still contain CO_2 (liquid +
830 vapor) and liquid H_2O at the cavity rim (see Raman spectrum in Fig. 5a). Sample INJ 34 (PPL). b)
831 Decrepitated CO_2 fluid inclusion trails within orthopyroxene. Large decrepitation aloes surround
832 single or groups of fluid inclusions (arrow). Sample INJ 7 PPL. c) Trail of CO_2 fluid inclusions in
833 olivine. Most inclusions appear dark and consist of talc/clinochlore + magnesite, having CO_2 and
834 H_2O reacted with olivine host. Around reacted inclusions, large yellowish aloes are present
835 (arrow). Sample INJ 34 PPL. d) Preserved $CO_2 \pm H_2O$ inclusions in olivine. Inclusions are
836 disposed along a transposed trail. Sample INJ 16 PPL. e) CO_2 fluid inclusions in clinopyroxene.
837 Amphibole inclusions of similar size are observed (arrow). Sample INJ 1. PPL. f) Back scattered
838 electron image showing fluid inclusion (black) and amphibole (dark gray) distribution in
839 clinopyroxene. Spinel inclusions and segregations are also visible (white). Sample INJ 16.
840 Fig. 5. Raman spectra of (a) H_2O in fluid inclusions in orthopyroxene, and of (b) clinochlore
841 (hydroxyls), (c) talc (hydroxyls), and (d) magnesite in reacted fluid inclusions in olivine.
842 Clinochlore hydroxyl vibrations at 3450, 3638, 3673 cm^{-1}, from Kleppe et al., 2003; the
843 additional vibration at 3565 cm^{-1} might be indicative for excess of Al, or for the additional

844 presence of humite (Frost et al., 2007). In spectrum d, non assigned peaks correspond to host
845 olivine.
846 Fig. 6. Histogram of homogenization temperatures to the liquid phase (Th) recorded in fluid
847 inclusions. Homogenization temperature intervals up to 50 °C were often registered within a
848 single inclusion trail. n = number of measurements.
849 Fig. 7. Synchrotron infrared imaging of water distribution in olivine and clinopyroxene from
850 deformed lherzolites. Each set of maps includes a microscopic image in plane polarized light,
851 and relative infrared maps in selected absorbance regions. *a*-*b*-*c*: a) investigated area in one
852 olivine grain. PPL. b) Absorbance map in the 3000 - 3600 cm^{-1} region and calculated water
853 contents in olivine (ppm). c) Qualitative distribution map of OH absorbance for clinochlore, talc,
854 and serpentine in the 3600 - 3800 cm^{-1} region , which allows to qualify hydrated phases in
855 olivine. *d*-*e*-*f*: d) Clinopyroxene not containing fluid inclusions. PPL. e) Absorbance map in the
856 3000 - 3800 cm^{-1} region and relative calculated water contents in clinopyroxene (ppm). f)
857 Qualitative OH absorbance map in the 3600 - 3800 cm^{-1} region relative to distribution of
858 amphibole inclusions. *g*-*h*-*i*: g) Clinopyroxene containing a trail of fluid inclusions. PPL. h)
859 Absorbance map in the 3000 - 3800 cm^{-1} region and relative calculated water contents in
860 clinopyroxene (ppm). i) Qualitative OH absorbance distribution map in the 3600 - 3800 cm^{-1}
861 region relative to distribution of amphibole inclusions. Sizes of investigated areas are in micron.
862 Measured water contents are drawn with a precision of 10's of ppm (see text). a.u. = arbitrary
863 units.
864 Fig. 8. Trace element composition of model aqueous fluids in equilibrium with clinopyroxene of
865 Injibara lherzolites. The trace element concentrations are normalized to primordial mantle (PM)
866 using the data from McDonough and Sun (1995). a) Trace element composition of model
867 aqueous fluids (pure H_2O, and brines - 5 molal NaCl solution) in equilibrium with clinopyroxene,
868 based on experimental partition coefficient data (Keppler, 1996; Ayers, 1998). b) Comparison of
869 model brine composition with trace element patters measured in Cl-rich fluid inclusions formed
870 at mantle depth; compositional range of slab-derived brines generated by antigorite
871 breakdown, from Scambelluri et al., 2002; carbonate-brine fluids in diamonds from peridotites
872 and eclogites, from Tomlinson et al., 2009.
873

Table 1

Representative chemical analyses of olivine, orthopyroxene and spinel

Sample	INJ16	INJ16	INJ16	INJ16	INJ16	INJ37	INJ4	INJ7	INJ16	INJ16	INJ35	INJ35	INJ4	INJ7	INJ16	INJ16
Mineral	Ol I	Ol II	Opx I av	Opx II av	Spl	Spl	Cpx core	Cpx core	Cpx rim	Cpx rim	Cpx core	Cpx core	Pargasite	Pargasite	Amp Fl	Amp Fl
Analyses	14ol39	23ol81	inj16opxC 2 analyses	inj16opxB 2 analyses	9spl8	72spl49	i4cpx49	i7cpx20	i16cpx15	i16cpx17	i35cpx12r	i35cpx64	i4amp24	i7amp22	21Amp136 EDS	21Amp139 EDS
SiO_2 wt%	40.94	40.91	55.67	55.8	0.07	0.04	52.6	52.76	52.51	52.21	52.41	52.62	42.81	42.97	42.1	41.97
TiO_2	< 0.01	< 0.01	0.11	0.11	0.2	0.14	0.47	0.56	0.53	0.58	0.45	0.54	2.54	2.46	2.45	2.73
Cr_2O_3	0.02	0.01	0.41	0.36	16.78	14.35	1.02	0.81	0.92	0.93	0.99	0.85	1.27	1.53	1.55	1.66
Al_2O_3	0.03	0.01	3.51	3.65	51.17	52.69	5.69	5.4	5.55	5.47	5.65	5.67	14.17	14.35	14.26	14.19
Fe_2O_3	0	0	0.53	0.76	2.16	2.21	0.88	0.37	0	0.1	0	0	4.88	4.63	4.56	4.36
FeO	10.52	10.2	6.02	5.75	10.83	9.63	1.97	2.74	2.78	2.77	3.08	3.03	0	0	0.35	0.35
MnO	0.12	0.17	0.16	0.15	<0.01	<0.01	0.05	0.07	0.04	0.03	0.02	0.14	< 0.01	< 0.01	< 0.10	< 0.10
MgO	48.79	49.14	33.23	33.51	19.25	19.7	15.65	15.54	15.12	15.37	15.18	15.06	17.21	17.5	17.33	17.31
NiO	0.51	0.31	0.06	0.12	0.32	0.4	0.03	0.07	0.06	< 0.01	0.03	0.01	0.1	0.2	< 0.10	< 0.10
CaO	0.05	0.02	0.62	0.59	< 0.01	0.01	20.48	20.27	20.11	20.24	20.27	20.17	10.4	10.44	11.34	11.15
Na_2O	< 0.02	< 0.02	0.09	0.06	< 0.02	< 0.02	1.54	1.52	1.46	1.46	1.45	1.52	3.99	4	3.7	3.82
K_2O	0.01	0.01	0.01	0.01	0.01	< 0.01	< 0.01	< 0.01	0.01	0.02	0.01	< 0.01	0.07	0.1	< 0.10	< 0.10
Cl	-	-	-	-	-	-	-	-	-	-	-	-	0.34	0.37	0.37	0.32
H_2O	-	-	-	-	-	-	-	-	-	-	-	-	2.03	2.04	2.11	2.11
Total	100.99	100.78	100.39	100.91	100.78	99.17	100.38	100.11	99.09	99.18	99.54	99.61	99.81	100.6	100.09	100.02
Cl=O							.	.	.	.	.	.	0.08	0.08	0.08	0.07
Total													99.73	100.51	100.02	99.94
Si a.p.f.u.	1	1	1.92	1.91	0	0	1.89	1.91	1.92	1.9	1.91	1.91	6.06	6.03	5.98	5.97
Al^{IV}	-	-	0.08	0.09	1.59	1.65	0.11	0.09	0.08	0.1	0.09	0.09	1.94	1.97	2.02	2.03
Al^{VI}	-	-	0.06	0.06	-	-	0.14	0.14	0.16	0.14	0.15	0.16	0.42	0.4	0.37	0.35
Ti	-	-	0	0	0	0	0.01	0.02	0.01	0.02	0.01	0.01	0.27	0.26	0.26	0.29
Cr	0	0	0.01	0.01	0.35	0.3	0.03	0.02	0.03	0.03	0.03	0.02	0.14	0.17	0.17	0.19
Fe^{3+}	0	0	0.01	0.02	0.04	0.04	0.02	0.01	-	-	-	-	0.52	0.49	0.49	0.47
Fe^{2+}	0.21	0.21	0.17	0.16	0.24	0.21	0.06	0.08	0.08	0.08	0.09	0.09	-	-	0.04	0.04
Mn	0	0	0	0	-	-	-	-	-	-	-	-	-	-	-	-
Mg	1.77	1.78	1.71	1.71	0.76	0.78	0.84	0.84	0.82	0.84	0.82	0.82	3.63	3.66	3.67	3.67
Ni	0.01	0.01	0	0	0.01	0.01	0	0	0		0	0	0.01	0.02	-	-
Ca	0	0	0.02	0.02	-	0	0.79	0.78	0.79	0.79	0.79	0.79	1.58	1.57	1.73	1.7
Na	-	-	0.01	0	-	-	0.11	0.11	0.1	0.1	0.1	0.11	1.1	1.09	1.02	1.05
K	0	0	0	0	0	-	-	-	0	0	0	-	0.01	0.02	-	-
Cl	-	-	-	-	-	-	-	-	-	-	-	-	0.08	0.09	0.09	0.08
OH	-	-	-	-	-	-	-	-	-	-	-	-	1.92	1.91	2	2
mg#	89.2	89.6	90.1	90.3	72.9	75.1	91	90	90.6	90.5	89.8	89.9	87.5	88.2	87.4	87.8
cr#	-	-	-	-	18	15										

EDS analyses of the tiny amphibole grains associated to fluid inclusions (Amp Fl) are reported for comparison. Ol I = porphyroclast; Ol II = neoblasts; Opx I = porphyroclast; Opx II = neoblast; Spl = spinel. mg# = Mg/(Mg+Fetot)*100; cr# (cr# = Cr/Cr+Al*100)

Table 2

Representative trace element analyses in clinopyroxene (Cpx) and amphibole (Amp)

Sample	INJ4	INJ7	INJ16	INJ16	INJ35	INJ35	INJ4	INJ7
Mineral	Cpx core	Cpx core	Cpx rim	Cpx rim	Cpx core	Cpx core	Pargasite	Pargasite
Analyses	i4cpx49	i7cpx20	i16cpx15	i16cpx17	i35cpx12r	i35cpx64	i4amp24	i7amp22
ppm								
Sc	82	62	95	105	74	73	44	42
V	250	261	243	245	230	238	354	378
Cr	-	-	-	-	-	-	8574	9361
Co	21.7	21.5	18.6	18.6	19.5	20	43.4	44.4
Ga	4	3	3	3	3	4	7	6
Rb	< 0.1	< 0.1	< 0.1	< 0.1	< 0.1	< 0.1	1.3	1.11
Sr	148	151	168	175	158	145	388	423
Y	17	12	21	22	20	19	19	16
Zr	38	25	43	47	40	41	31	26
Nb	< 0.1	0.5	< 0.1	< 0.1	< 0.1	< 0.1	8	10.7
Cs1	< 0.1	< 0.1	< 0.1	< 0.1	< 0.1	< 0.1	< 0.1	< 0.1
Ba	<0.4	13	<0.4	<0.4	<0.4	2	285	356
La	7.3	6.8	9.6	9	7.5	7.3	8.3	8.3
Ce	10	12	12	12	10	9	13	15
Pr	1.2	1.3	1.6	1.6	1.1	1.1	1.4	1.6
Nd	6	6	8	8	7	6	7	7
Sm	1.9	1.6	2.6	2.7	2.1	2.1	2.2	1.9
Eu	0.65	0.64	0.91	0.95	0.99	0.83	0.93	0.79
Gd	2.4	2.2	2.9	3.1	3.3	3.2	3.2	2.7
Tb	0.39	0.29	0.56	0.48	0.52	0.47	0.51	0.44
Dy	3.5	2.5	4.2	3.7	3.4	3.6	3.5	3
Ho	0.63	0.47	0.86	0.77	0.75	0.79	0.78	0.56
Er	2.2	1.5	2.5	2.5	2.2	2.3	2	1.7
Tm	0.3	0.19	0.29	0.37	0.26	0.33	0.32	0.27
Yb	2	1.3	2.2	2.2	1.8	2	1.7	1.6
Lu	0.29	0.19	0.29	0.33	0.22	0.29	0.29	0.21
Hf	1.2	0.7	1.2	1.3	1.5	1.3	0.7	0.7
Ta	0.03	0.04	< 0.009	0.04	< 0.009	< 0.009	0.3	0.53
Pb	2.3	2.8	1.9	1.9	2.1	3.1	9	10.5
Th	0.75	0.56	0.89	0.93	0.78	0.74	0.69	0.67
U	0.18	0.17	0.16	0.18	0.19	0.18	0.19	0.23
K	< 83	< 83	83	166	83	< 83	582	831
Ti	2818	3357	3177	3477	2698	3237	15227	14748

Table 3
Summary fluid inclusion properties

Petrography

Host phase	Composition		Textural characteristics			liquid H_2O detection			
	Preserved	Reacted	Size (µm)	Distribution	Abundance	Optical	Microtherm.	Raman	IR
Ol I	CO_2 ± H_2O	Mg-chlorite (Talc) + Magnesite	<3 - 30	early in porphyroclasts	present in most grains	no	yes	yes	yes
Opx I	CO_2 ± H_2O	no	<3 - 60	early in porphyroclasts	present in most grains	yes	yes	yes	yes
Cpx	CO_2	-	<3 - 30	early with amphibole	rare	no	no	no	no

Microthermometry of H_2O - CO_2 inclusions

Sample	Host phase	Tf_{CO2} Tf°C	Tm_{CO2} °C	Th_{CO2} °C	Tf_{H2O} °C	Te °C	Tm_{Hhl} °C	Tm_{Clat} °C	Salinity NaCl eq.wt.%
INJ7/6A	Opx I	-89.2	-56.4	30.5	-51.3	-33.2	-11.3		
INJ7/6A	Opx I	-88.9	-56.4	27.2	-50.4	-31.6			
INJ7/7B	Opx I	-72.3	-56.3	6.4	-51.8	-30.7		5.6	10
INJ23/1A	Ol I	-69.9	-57.6	24.2				2.7	14
INJ23/1A	Ol I	-72.5	-56.7	24				2.7	14
INJ23/1A	Ol I	-72.8	-56.7	23.9				2.7	14

Ol I: olivine porphyroclast; Opx I: orthopyroxene porphyroclast; Cpx: clinopyroxene; Microtherm.: Microthermometry; Tf = Temperature of freezing; Te = Eutectic Temperature; Tm = Temperature of melting; Th = Temperature of homogenization to the liquid phase; Hhl: hydrohalite; Clat = clathrate

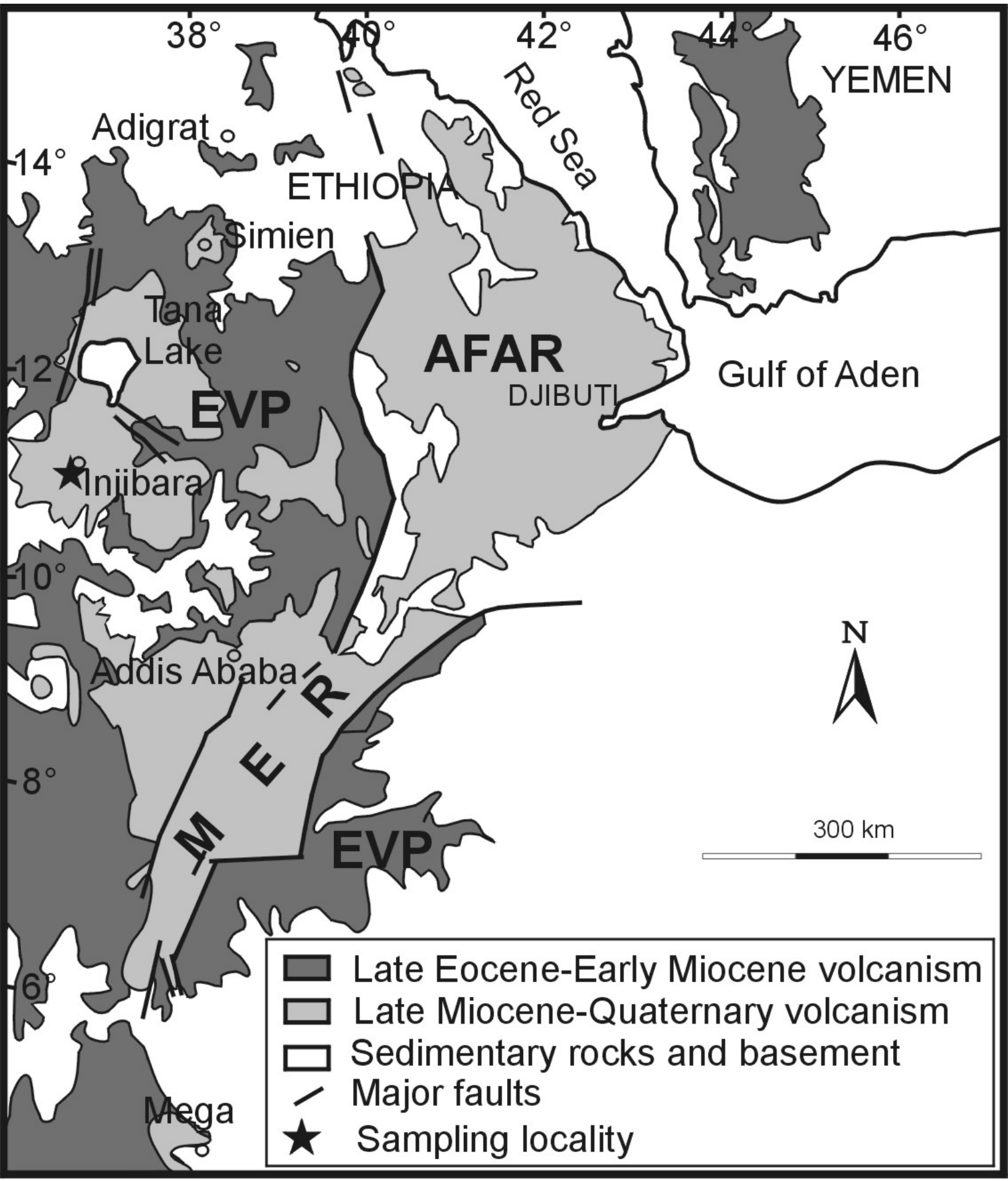
38°
40°
42°
44°
46°
YEMEN
Red Sea
Adigrat
14°
ETHIOPIA
Simien
Tana
Lake
12°
AFAR
DJIBUTI
Gulf of Aden
EVP
Injibara
10°
N
Addis Ababa
M E R
8°
300 km
EVP
6°
Mega
Late Eocene-Early Miocene volcanism
Late Miocene-Quaternary volcanism
Sedimentary rocks and basement
Major faults
Sampling locality

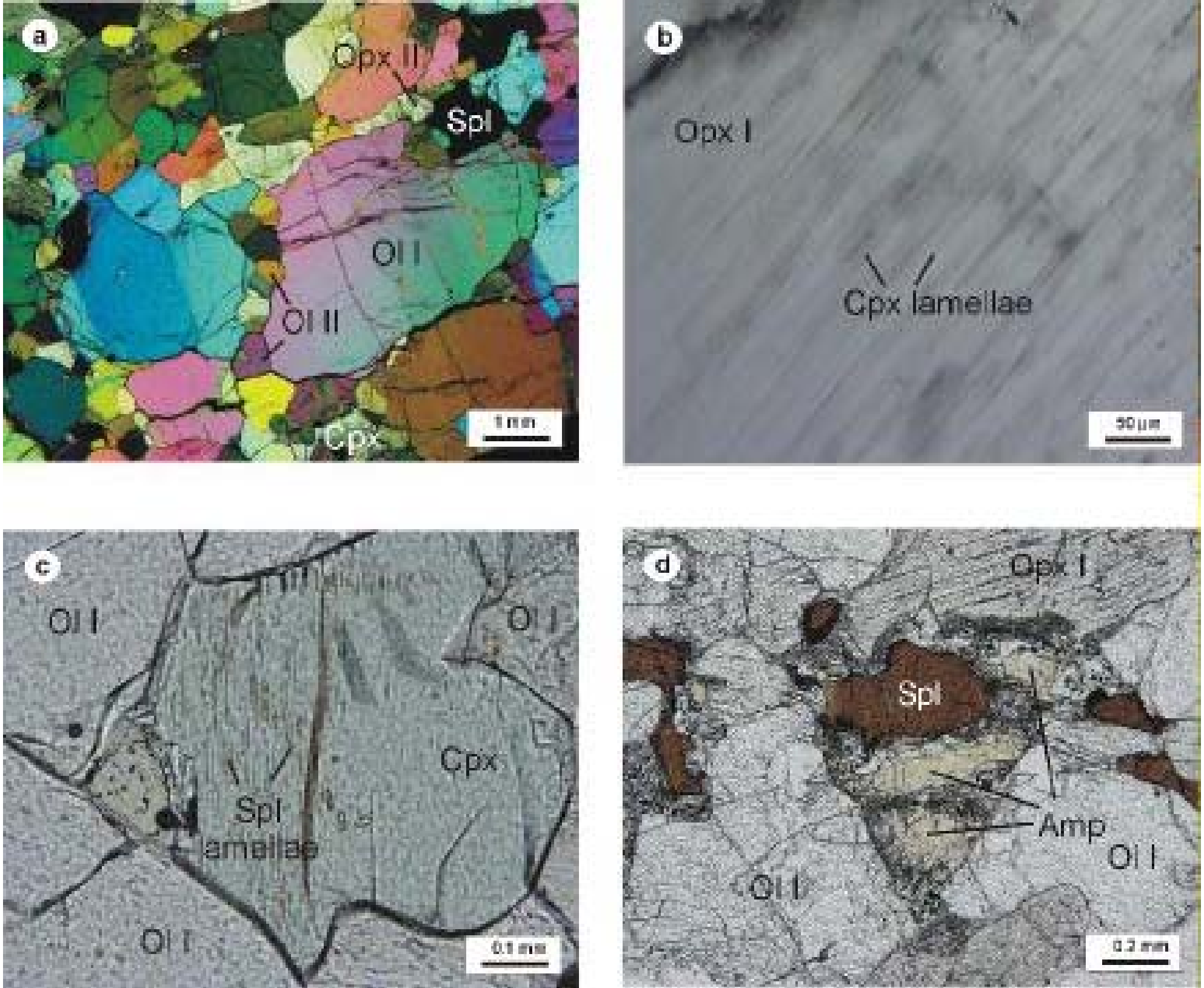
a
Opx II
Spl
Ol I
Ol II
Cpx
1 mm
b
Opx I
Cpx lamellae
50 µm
c
Ol I
Ol I
Cpx
Spl
lamellae
Ol I
0.1 mm
d
Opx I
Spl
Amp
Ol I
Ol I
0.2 mm

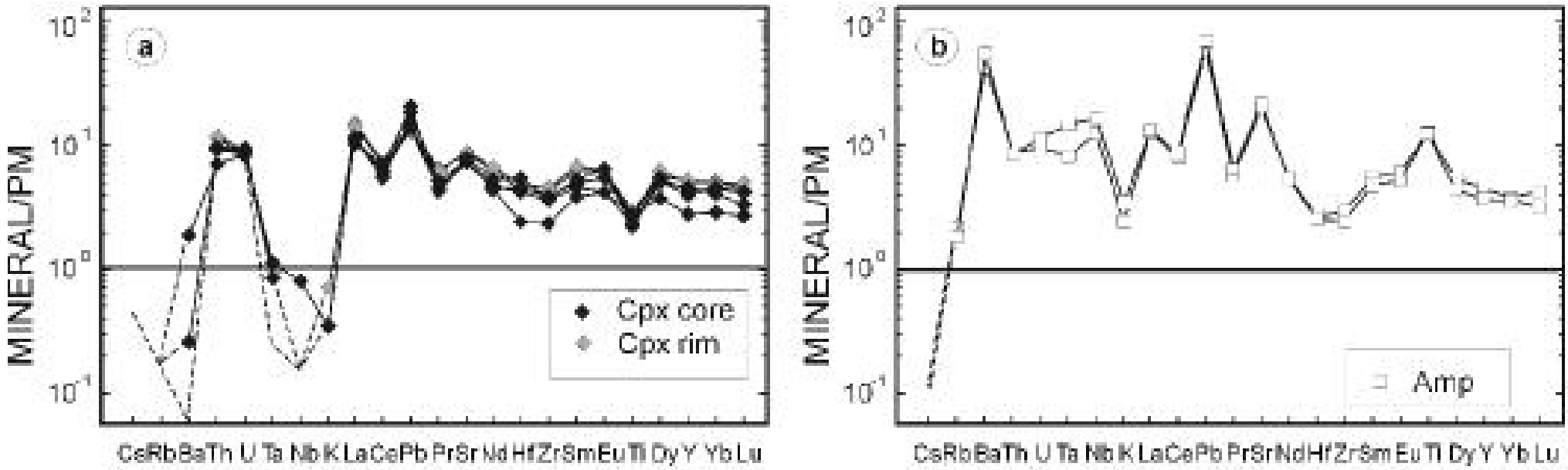
a
b
MINERAL/PM
10^2
10^1
10^0
10^{-1}
Cpx core
Cpx rim
Amp
CsRbBaTh U Ta Nb K LaCePb PrSr Nd Hf Zr Sm Eu Ti Dy Y Yb Lu

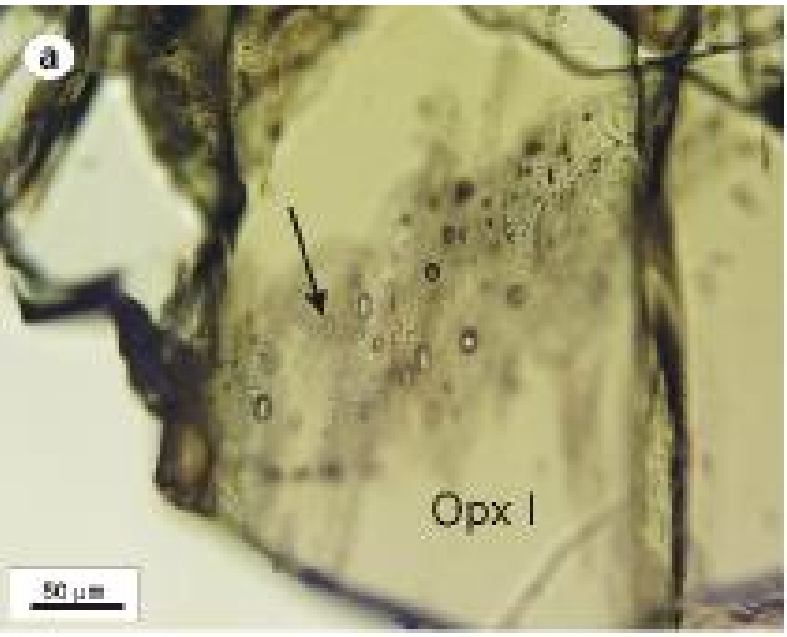
a
Opx I
50 µm

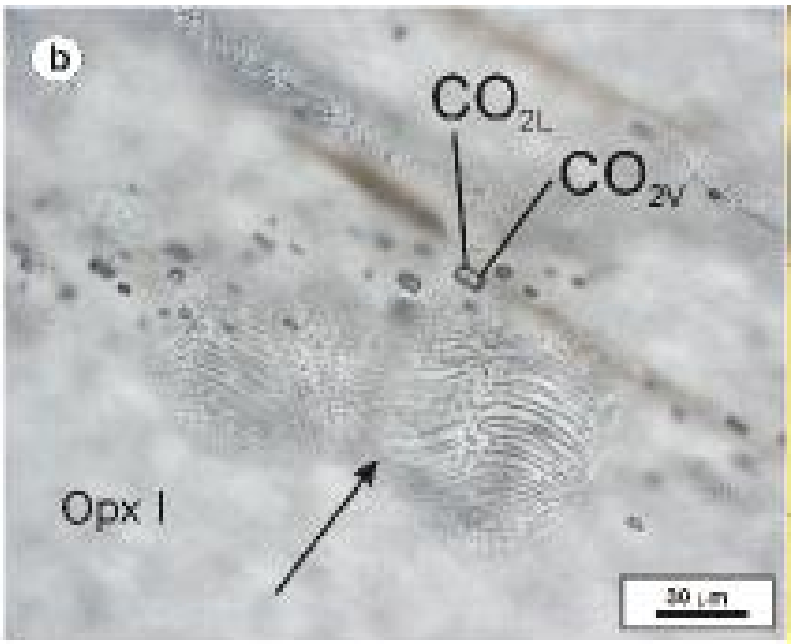
b
CO_{2L}
CO_{2V}
Opx I
30 µm

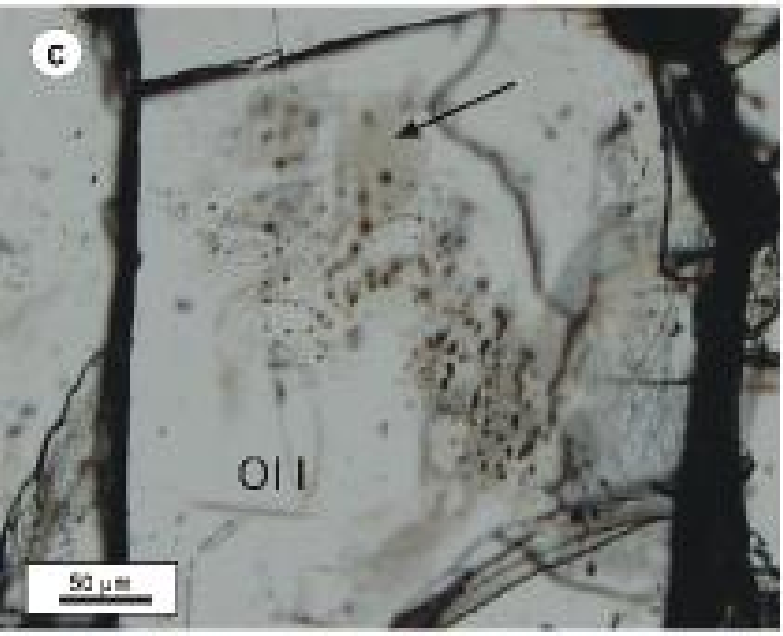
c
Ol I
50 µm


d
Ol I
30 µm

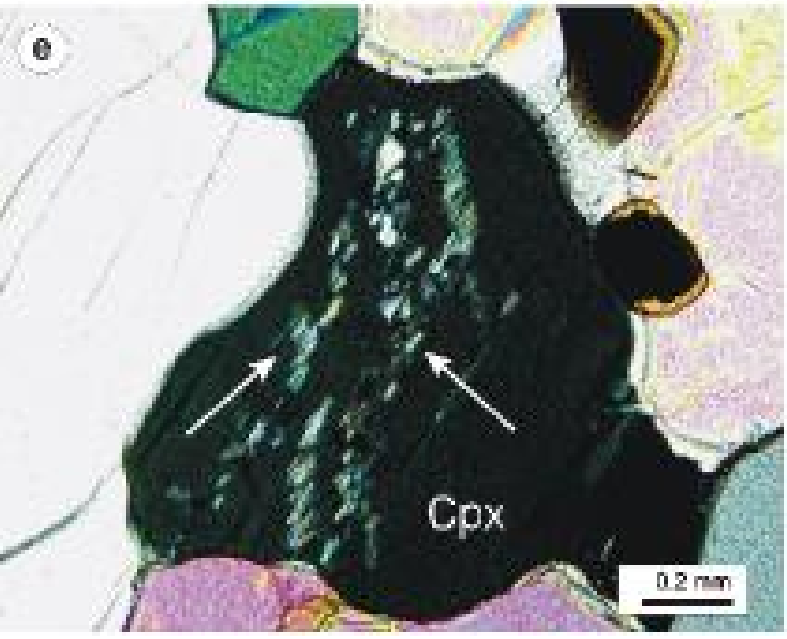
e
Cpx
0.2 mm

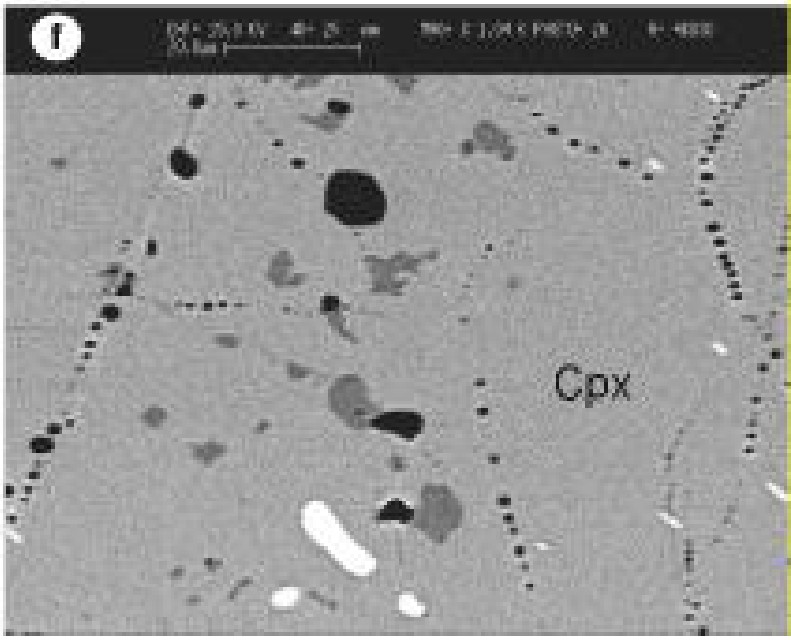
f
Cpx

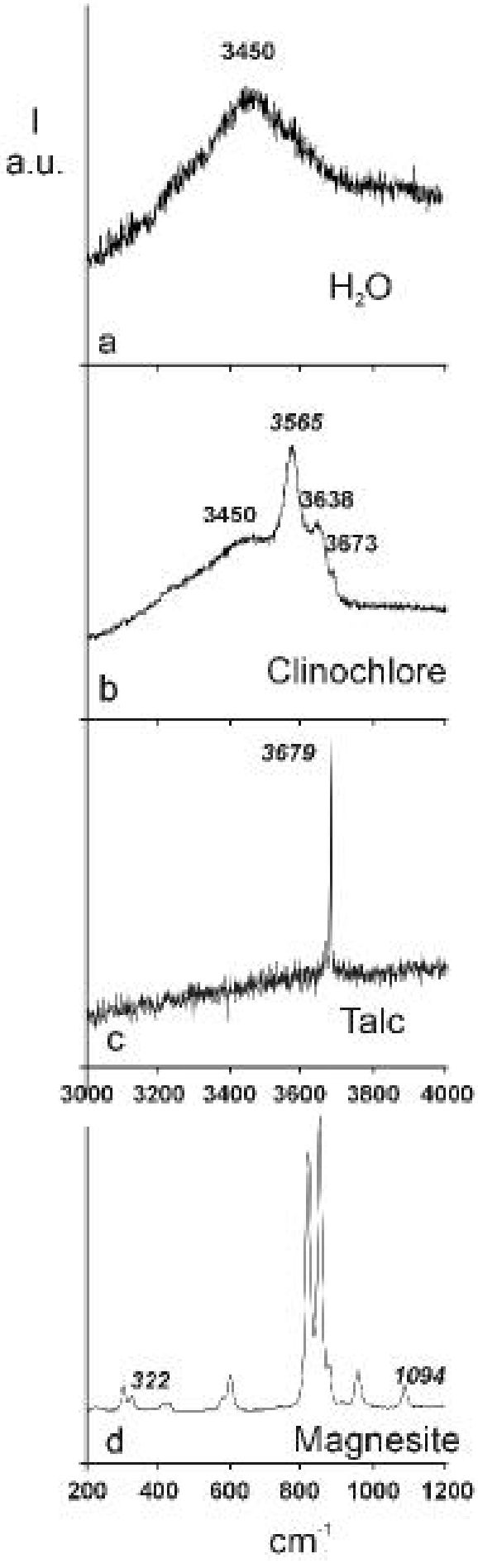
3450
I
a.u.
H2O
a
3565
3450
3638
3673
b
Clinochlore
3679
c
Talc
3000 3200 3400 3600 3800 4000
322
1094
d
Magnesite
200 400 600 800 1000 1200
cm-1

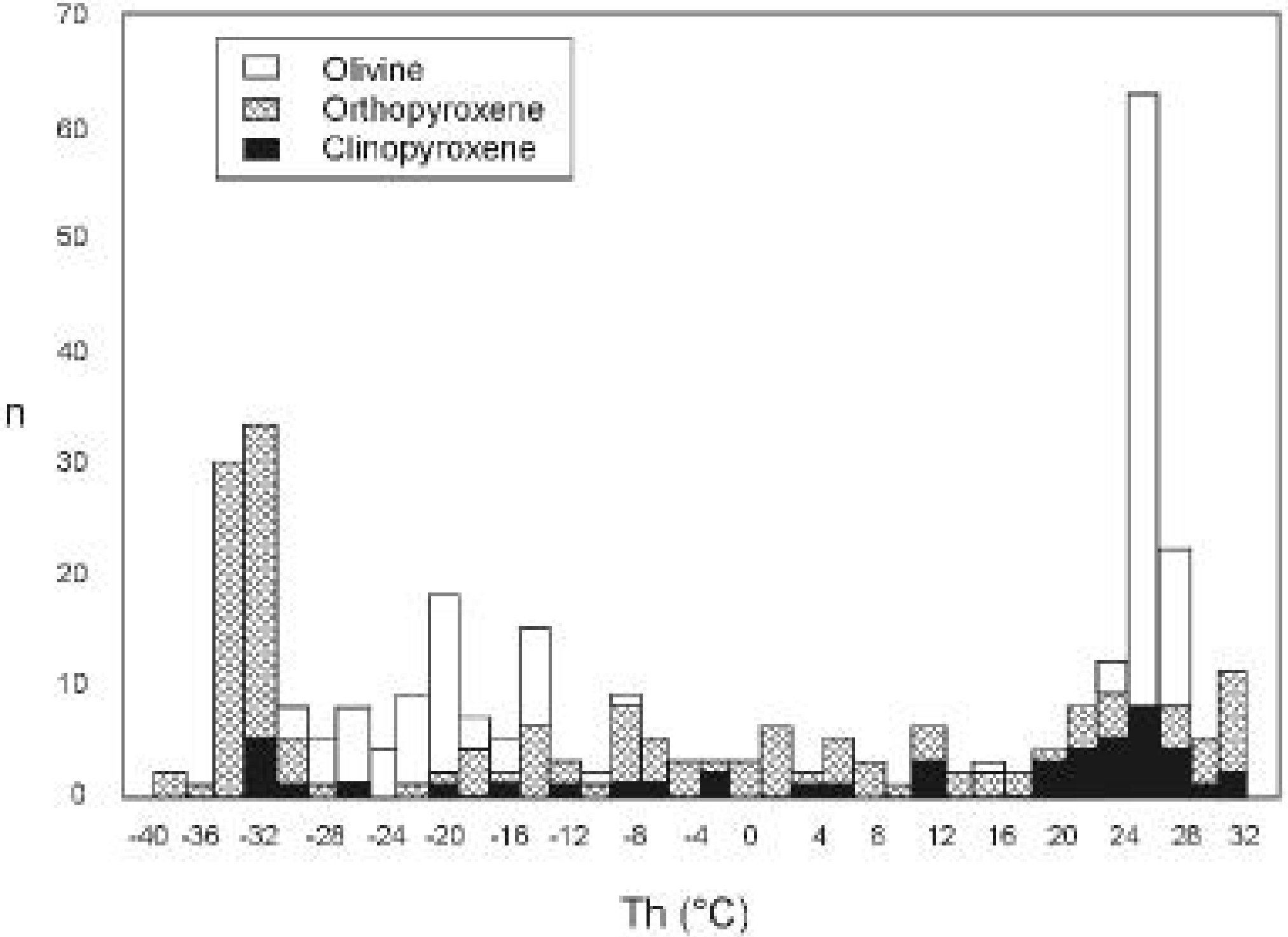
Olivine
Orthopyroxene
Clinopyroxene
n
70
60
50
40
30
20
10
0
-40
-36
-32
-28
-24
-20
-16
-12
-8
-4
0
4
8
12
16
20
24
28
32
Th (°C)

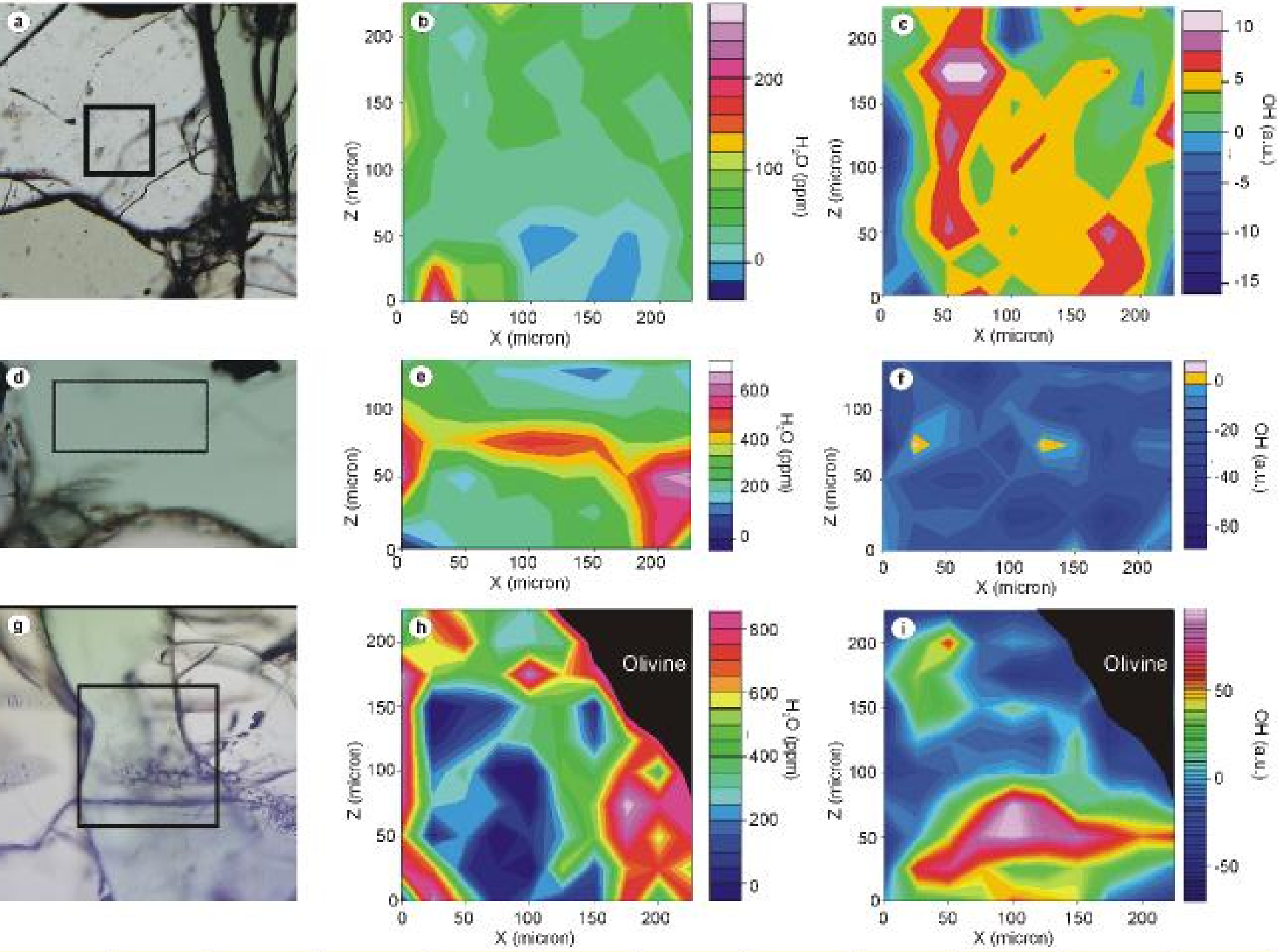
a
b
c
d
e
f
g
h
i
Olivine
Olivine
Z (micron)
X (micron)
H2O (ppm)
OH (a.u.)
0
50
100
150
200
400
600
800
10
5
-5
-10
-15
-20
-40
-60
-50

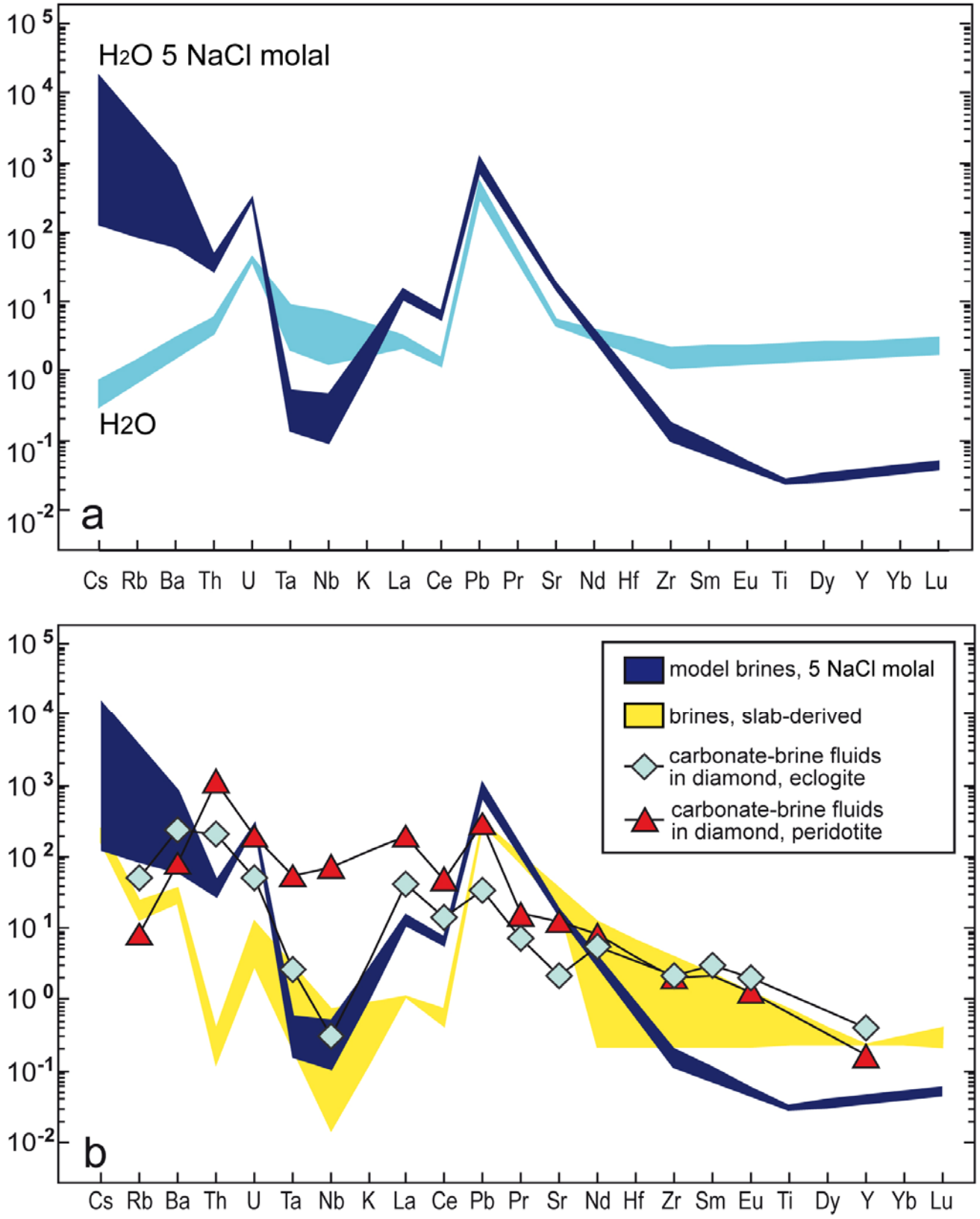
H2O 5 NaCl molal
H2O
a
10 5
10 4
10 3
10 2
10 1
10 0
10-1
10-2
Cs Rb Ba Th U Ta Nb K La Ce Pb Pr Sr Nd Hf Zr Sm Eu Ti Dy Y Yb Lu

model brines, 5 NaCl molal
brines, slab-derived
carbonate-brine fluids in diamond, eclogite
carbonate-brine fluids in diamond, peridotite
b
10 5
10 4
10 3
10 2
10 1
10 0
10-1
10-2
Cs Rb Ba Th U Ta Nb K La Ce Pb Pr Sr Nd Hf Zr Sm Eu Ti Dy Y Yb Lu

Fig. 8